# Università degli Studi di Ferrara

DOTTORATO DI RICERCA IN

"FARMACOLOGIA E ONCOLOGIA MOLECOLARE"

CICLO XXIV

COORDINATORE Prof. Antonio Cuneo

# Role and regulation of miR-483 in cancer

Settore Scientifico Disciplinare BIO/11

**Dottorando**
Dott. Veronese Angelo

**Tutore**
Prof. Carlo Maria Croce

Anni 2008/2011

# INDEX

**Abstract**

The *hsa-mir-483* locus is located at chromosome 11p15.5 within intron 2 of the *IGF2* locus. Because of its location, de-regulated in Wilms' tumor and other neoplasia, I hypothesized that this microRNA had a potential role in tumors. By analyzing 19 Wilms' tumors, I proved that *miR-483-3p* is indeed over-expressed in 100% of the cases and a co-regulation with the over-expression of *IGF2* was found.

However, several other types of common adult cancers exhibit high or even extremely high levels of *miR-483-3p* expression without *IGF2* over-expression. Indeed, independently from *IGF2*, the expression of the *miR-483-3p* could also be induced by the oncoprotein β-catenin through a novel interaction with the basic Helix-Loop-Helix protein upstream stimulatory transcription factor 1 (USF1).

I also show that β-catenin itself is a target of *miR-483-3p,* triggering a negative regulative loop that becomes ineffective in cells harbouring activating mutations of β-catenin pathway.

The potential oncogenic role of *miR-483-3p* was supported by the findings that its ectopic expression protects cells from apoptosis and, conversely, its inhibition increase the level of apoptosis. To understand the mechanisms of its action, I investigated potential gene targets. Among these, an important pro-apoptotic protein, Puma, were inhibited by *miR-483-3p*. My results indicate that *miR-483-3p* functions as an anti-apoptotic oncogene, coordinately over-expressed with *IGF2* in Wilms' tumors or induced by β-catenin activation in other tumor types.

**Significance**

IGF2 is a fetal growth factor where abnormally high expression has been associated with the Beckhwith-Wiedeman syndrome that predisposes to the development of nephroblastoma, hepatoblastoma and rhabdomyosarcoma. Here I show that *miR-483-3p,* located within intron 2 of *IGF2* gene, is overexpressed in all the Wilms' tumors I studied. I also show this microRNA target a proapoptotic protein, Puma, and behave as an antiapoptotic oncogene. Moreover I demonstrate that dysregulation of *miR-483-3p* can also occur independently of *IGF2* dysregulation. In this case miR-483-3p is regulated by β-catenin oncogene and may contribute to its antiapoptotic activity.

## Introduction

Genetic and epigenetic abnormalities at chromosomal region 11p15.5 have been associated with various human neoplasms and with the cancer-predisposing Beckwith-Wiedeman syndrome (BWS). In particular, loss of alleles and gene duplication at 11p15 are typically detected in more than 80% of Wilms' tumors [1-5] and, albeit less frequently, in more common adult neoplasms [6-9].

Two close imprinted loci, that harbor at least eight mono-allelically expressed genes, are present at chromosome region 11p15.5. The aberrant regulation of genomic imprinting at 11p15.5 was involved in human cancer [10-12]. Aberrant methylation at the *H19* maternal locus leads to the reactivation of the silent *IGF2* allele [10,13-16] and the loss of maternal allele methylation at the *KvDMR1* locus was linked to reduced expression of the cyclin-dependent kinase inhibitor *CDKN1C/p57* gene and other imprinted genes [11,12,17-19]. These studies point to the existence of oncogenic, *IGF2*, as well as tumor suppressive, *CDKN1C/p57*, functions within the 11p15.5 chromosomal imprinted region.

IGF2 is a fetal growth factor, whose abnormal expression has been involved in the Beckwith-Wiedemann syndrome, which predisposes to the development of nephroblastoma, hepatoblastoma, and rhabdomyosarcoma. Biallelic expression of *IGF2* gene, consequent the loss-of-imprinting (LOI) at the *IGF2* locus, occur in 40-50% of Wilms' tumor [5,20] and it is thought to be an early event in carcinogenesis. So it has been suggested that increased IGF2 could lead to an enhanced cellular proliferation, differentiation failure and tumor development. However, a transgenic mouse model for *IGF2* over-expression exhibited many of the features associated with the Beckwith-Wiedemann syndrome, including prenatal overgrowth, polyhydramnios, fetal and neonatal lethality, disproportionate organ overgrowth including tongue enlargement, and skeletal abnormalities, but did not develop tumors [21]. These results suggest that additional cofactors cooperate with IGF2 in promoting human cancer. Recently, the *IGF2* locus was shown to harbor a miRNA, the *mir-483* locus, within its second intron [22].

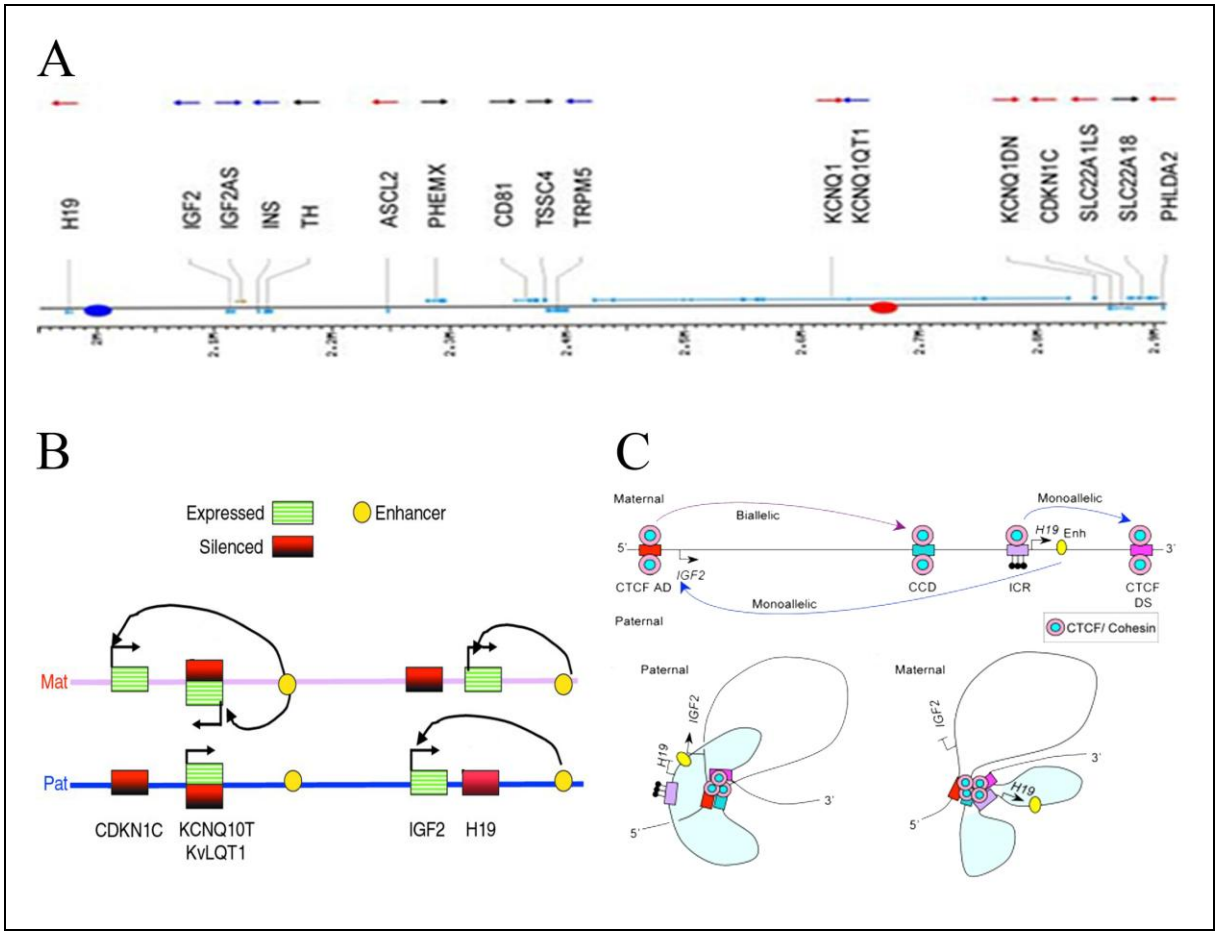


**Fig.1 Genomic structure of the 11p15.5 chromosome region and its imprinted genes**.(A) Location of the genes mapping in the 11p15.5 chromosome region and their imprinted status. Red arrows, on the top of the panel, indicate the maternal allele expression, blue arrows the paternal allele expression whereas black arrows indicate the biallelic expression. (B) Simplified model of the imprinted status of the CDKN1C/KCNQ10T/KvLQT1 and IGF2/H19 genes imprinted locus (from J Clin Invest. 2000;105(3):247–252). (C) Schematic representation of the tridimensional structure obtained by the interaction between CTCF-Cohesin, other proteins to permit the monoallelic expression of the IGF2 and H19 genes. DNA elements are indicated as follows: CTCF AD (red bar); ICR (purple bar), and CTCF DS (Cerise bar), Enhancer is yellow oval. Pink and pale blue ovals represent the CTCF/cohesin complexes. CpG methylation is depicted as filled lollipops. On the paternal allele, co localisation of CTCF and cohesin at CTCF AD, and CTCF DS brings these regions together. The methylated ICR does not bind CTCF and is thus excluded from CTCF/cohesin interacting regions. The exclusion of the ICR may enable the IGF2 gene promoters and H19 enhancer region to interact, (shown by yellow oval close to IGF2 arrow) even though they are on different looping domains. (The H19 domain is shaded.) On the maternal allele, CTCF/cohesin can bind to the unmethylated ICR which can then interact with other CTCF/cohesin sites.

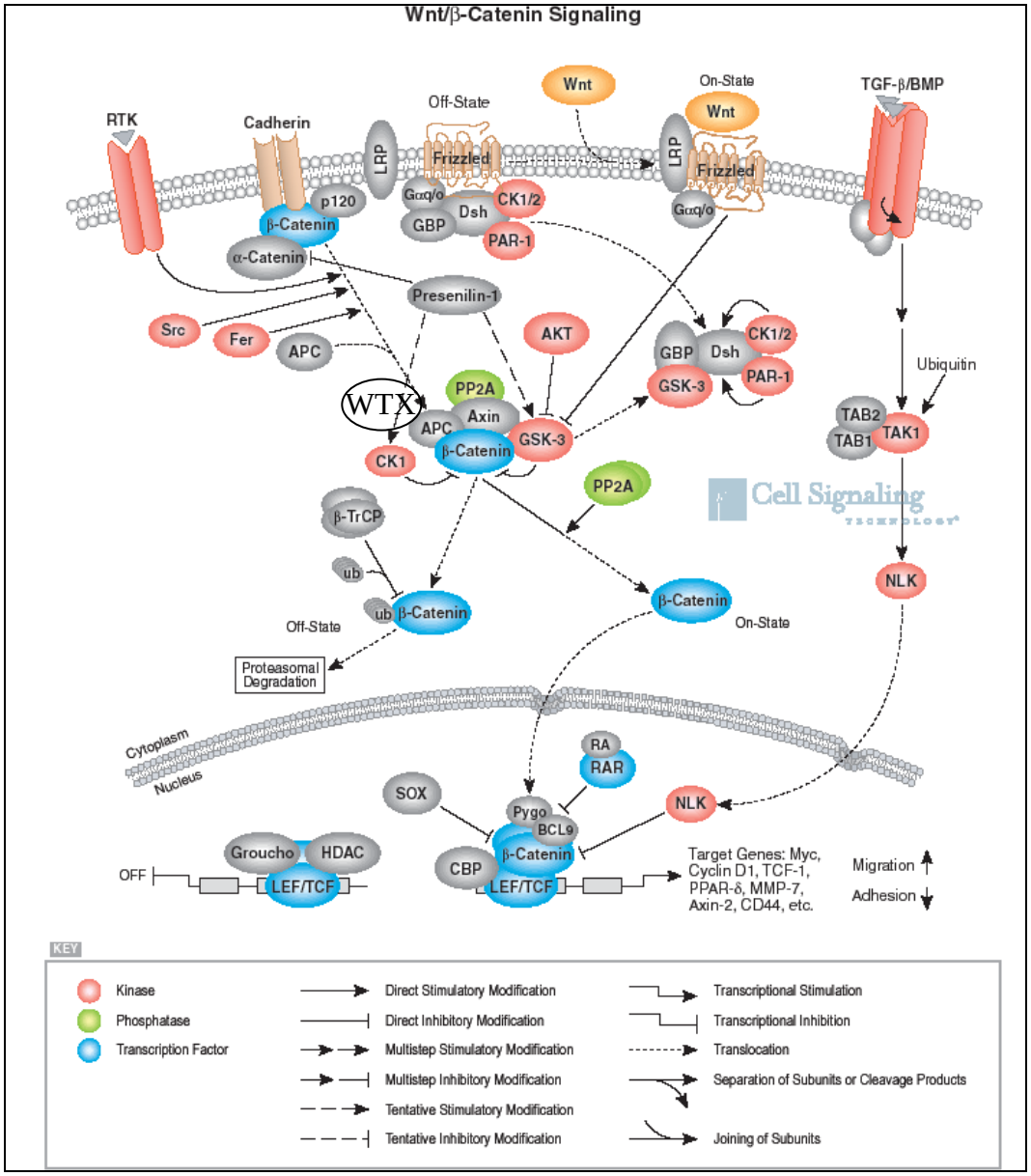


**Fig.2 Wnt/β-catenin signaling** (from Cell signaling technology, http://www.cellsignal.com). The figure show how β-catenin (blue oval) could be part of the membrane E-Cadherin/α-catenin complex, compounded to the APC/Axin/GSK3β/WTX complex for its degradation or be in the nucleus to act as a transcription factor. Every step of this pathway could be regulated by numerous protein/enzyme where the most important is by the Wnt-Frizzled molecules able to block the β-catenin degradation by the APC/Axin/GSK3β complex.

β-catenin is a multifunctional protein involved in cell-cell adhesion when it is localized to the cellular membrane [23], and in transcriptional regulation by translocation into the nucleus through the Wnt pathway [24]. Wnt signaling is an important molecular pathway required for cellular differentiation, tissue homeostasis, and tissue morphogenesis. Wnt/β-catenin signaling is one of the most commonly activated pathways in cancer and several Wnt signaling related gene mutations have been described: adenomatous polyposis coli (APC)

and protein phosphatase 2 regulatory subunit A (PPP2R1B) mutations in colorectal cancer [25], axin1 mutation in hepatocarcinoma [26], WTX gene mutations in Wilms' tumor [27] and β-catenin gene (CTNNB1) itself was shown to be mutated [28-30] in the amino terminal region employed for degradation by the GSK3β -APC-Axin-WTX complex [27,31]. These mutations prevent β-catenin degradation and result in its accumulation in the nucleus where it acts as a specific transcriptional co-activator of the DNA binding T cell factor/lymphoid enhancer factor protein family (TCF/LEF). Among the targets of this family are important genes involved in tumorigenesis such as MYC, CCND1, CJUN and FRA1. [32,33] (**Fig.2)**.

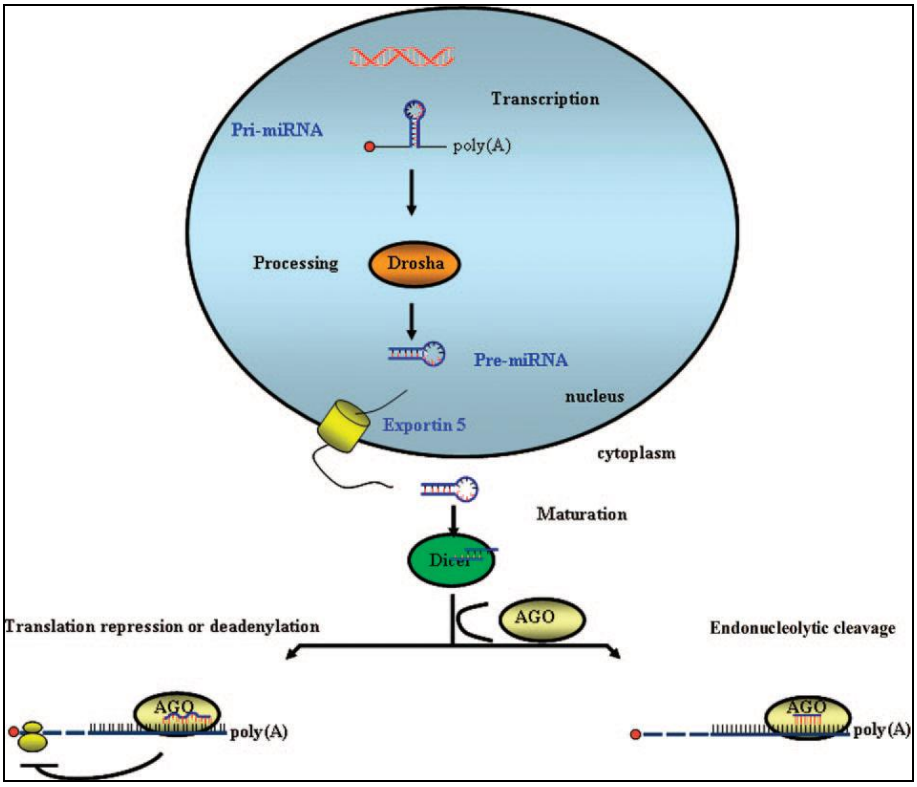


**Fig.3 Biogenesis of miRNAs and assembly into protein complexes**. miRNA precursor molecules (pri-miRNAs) fold into hairpin structures that contain imperfect base-paired stems in a two-step process catalyzed by two different RNase III-type endonucleases. Drosha first cleaves pri-miRNAs,forming _70 nucleotide hairpins (pre-miRNAs) in the nucleus. Subsequently, pre-miRNAs are transported to the cytoplasm by Exportin 5, where they are cleaved by Dicer to yield _20-bp miRNA duplexes. After processing, miRNAs are assembled into RNP (ribonucleic protein) complexes, called miRNPs, with proteins of the AGO family. miRNPs tether to the 3_UTR of a mRNA target to repress protein synthesis. In the case of perfect bp alignment, the miRNP complex cleaves the duplex miRNAmRNA; however, multiple mechanisms [34] are used on duplex miRNA:mRNA with imperfect complementary.

MicroRNAs (miRNAs) are small non-coding RNAs that modulate gene expression by base pairing to the target messenger RNAs (mRNAs) and by inhibiting their translation and/or promoting their degradation [35] (**Fig.3**). MicroRNAs play a critical role in the normal maintenance of fundamental cellular processes and their deregulation in human neoplasm has been proven to affect a large number of molecular pathways related to cancer [36-38]. Indeed

microRNA aberrant expression of miRNAs has been detected in any human neoplasm and miRNAs were found to play a central role in all molecular pathways affecting cancer traits [36,38,39]. Since the *miR-483* locus is dysregulated in tumors involving the β-catenin pathway [40-42] I investigated also their possible connection. Here I demonstrate that expression of *miR-483* can be induced independently of its host gene IGF2 by the oncoprotein β-catenin through a novel interaction with the basic Helix-Loop-Helix protein upstream stimulatory transcription factor 1 (USF1) . I also show that β-catenin itself is a target of *miR-483-3p,* triggering a negative regulative loop that becomes ineffective in cells harbouring activating mutations of β-catenin pathway.

Therefore, I illustrate the potential oncogenic activity of *miR-483-3p,* one of the mature products of the *hsa-mir-483* locus, which is located within the *IGF2* locus at chromosome 11p15.5. My results provide evidences for a role of this miRNA as an anti-apoptotic oncogene, which may cooperate with IGF2 in tumorigenesis.

## Materials and Methods

**Primary tumors**. Primary tumor RNAs were obtained from 19 Wilms' tumor, 3 adjacent patient normal tissues, 2 adult kidneys; 27 hepatocarcinoma (HCC), 7 cirrhotic and 2 normal liver tissues; 23 colorectal cancers (CRC) and 5 normal colon mucosa; 19 breast cancers (BrCa) and 4 normal breast tissues. All tissue samples were collected at surgery, immediately snap frozen in liquid nitrogen, and stored at -80°C until RNA extraction. Total RNA was isolated using Trizol (Invitrogen) according to manufacturer's instructions.

**Cell lines and transfection**. HEK293 (ATCC number CRL-1573), HepG2 (ATCC number HB-8065), HCT116 (ATCC n. CCL-247) cell lines were cultured with Iscove's modified Dulbecco's medium with 10% fetal bovine serum. *hsa-miR-483-3p* precursor (Sanger accession MI0002467) and Negative control 2 ribo-oligonucleotide were from Applied Biosystems/Ambion. Anti-microRNA oligonucleotides (AMOs) against *miR-483-3p* and against the GFP gene (AMO Negative Control) were from Fidelity Systems (Gaithersburg MD, USA). RNA interfering for BBC3/PUMA and scramble control were from Santa Cruz (Santa Cruz, CA). . siRNA for MYC (cat. L-003282-00-0005), CTNNB1 (cat. L-003482-00) and scramble negative control (cat. D-001810-10-20) were from Dharmacon. Transfection of miRNAs, AMOs and expression vectors was carried out with lipofectamine 2000 (Invitrogen, cat. 116688-019) in accordance with manufacturer's procedure.

**Luciferase assays and vectors**. The human 3'UTRs of BBC3/PUMA and CTNNB1 were amplified by PCR using the primers indicated in **Table 1** and cloned downstream of the firefly luciferase gene in the pGL3-Control vector (Promega). Substitutions into the miR-483-3p binding sites of the 3'UTR genes were introduced by using Quick-Change Site direct Mutagenesis Kit (Stratagene, CA, USA) following the manufacturer's instructions using the primers indicated in **Table 1**. As a reference, the pRLTK vector (Promega), which expresses the renilla luciferase, was used. Transfection was conducted in HEK293, HCT116 and HepG2 cells cultured in 24-well plates, each well was cotransfected with 400 ng of pGL3-control vectors together with 40 ng of pRLTK reference vector (Promega) and 30 pmol of *miR-483-3p* or Negative control 2 or AMOs or methylated control oligonucleotide. Twenty-four hours after transfection, *firefly* and *renilla* luciferase activities were measured using the Dual-Luciferase Report Assay (Promega). β-catenin and USF1 expression vectors were generated cloning β-catenin cDNA and USF1 cDNA into the pIRES-Neo2 (Clontech), and pCMV-Tag (Agilent Technologies) vectors see **Table 2** for primers sequences. To test the β-catenin nuclear activity, the pGL3-OT and pGL3-OF luciferase responsive vectors were used

[43]. pGL3-OT is a TCF-LEF responsive reporter, pGL3-OF is a negative control with a mutated TCF-LEF binding site. Each transfection was repeated at least twice in triplicate. To analyze the promoter of the miR-483 I used the pGL4 luc2 .1 (Promega) where I cloned the SV40 enhancer downstream the luciferase gene.

**Western blots analysis.** HEK293, HepG2 and SW480 cell lines were transfected with 30 pmol of *miR-483-3p*, AMOs and controls sequences in 24-well plates. After 48 hours cells were collected, lysed in Laemmli 2X buffer and analyzed by western blot to assess the expression of PUMA using monoclonal antibodies (Cell Signaling, anti-PUMA antibody #4976). Primary antibody was incubated 2 hours at room temperature and then peroxidase conjugated anti-mouse or anti-rabbit antibodies were incubated 30 minutes at room temperature. Detection was conducted by chemiluminescent enhanced assay (WesternBreeze Chemiluminiscent Kit cat. WB7104, Invitrogen). β-actin antibody (Cell Signaling, β-Actin Antibody #4967) or Ponceau staining were used to normalize protein loading. To quantify western blot signals, digital images of autoradiographies were acquired with Fluor-S MultiImager, and band signals were quantified in the linear range of the scanner using specific densitometric software (Quantity One).

**RNA isolation and Quantitative Real time RT-PCR (qRT-PCR).** Purification of total RNA using TRIzol reagent (Invitrogen, Carlsband, CA, USA) was carried out following the manufacturer's instructions. Mature microRNA expression was assayed by Taqman MicroRNA assay (Applied Biosystem) specific for *miR-483-3p* (P/N: 4378094) and normalized on RNU6B (P/N: 4373381). Five ng of total RNA was reverse transcribed using the specific looped primer and real time quantitative PCR was conducted using the standard Taqman MicroRNA assay protocol on a Biorad-Chromo4 thermal cycler. The 20 μL PCR included 1.33 μL reverse transcription product, 1X Taqman Universal PCR Master Mix, No AmpErase UNG (P/N 4324018 (Applied Biosystem), 0.2 μmol/L Taqman probe, 1.5 μmol/L forward primer, 0.7 μmol/L reverse primer. The reaction was carried out in a 96-well PCR plate at 95°C for 10 min followed by 40 cycle of 95° C for 15 sec and 60°C for 1 min. Each sample was analyzed in triplicate. qRT-PCR for mRNAs was performed using 500 ng of total RNA for each sample according to the manufacturers' instruction (High capacity cDNA Reverse Transcription Kit, Applied Biosystems) and the real time reaction using SYBR green technologies (Power SYBR green PCR Master Mix, Applied Biosystems) on the Biorad-Chromo4 instrument. The 20 μL PCR included 1 μL reverse transcription product, 1X Power SYBR green PCR Master Mix, (P/N 4368577, Applied Biosystem), 0.4 μmol/L forward

primer, 0.4 μmol/L reverse primer. The reactions were incubated in a 96-well PCR plate at 95° C for 10 min followed by 40 cycle of 95° C for 15 sec and 60° C for 1 min. Each sample was analyzed in triplicate. TaqMan gene expression assays was performed for *IGF2, BBC3/PUMA and CDKN1A/P21,* primiR-483 genes using primers and probes (Hs01005963_m1, Hs00248075_m1, Hs99999142_m1) obtained from Applied Biosystems (Applied Biosystems, Foster City, CA). The expression of 18S RNA was used as endogenous reference control. ). To avoid genomic contamination in the quantification of the IGF2 intron 2 and primiRNA-483 RNA samples were previously treated with DNAse (TURBO DNA-free™ Kit, cat. AM1907, Ambion). The list of primers that I used herein is shown in **Table 2**. The level of miRNA and mRNA were measured using Ct (threshold cycle). The amount of target, normalized to an endogenous reference and relative to a calibrator, is given by: $2^{-\Delta\Delta Ct}$ (Comparative Ct method, Applied Biosystem User Bulletin #2).

**Northern blot analysis.** RNA samples (10 μg each) were electrophoresed on 15% acrylamide and 7 mol/L urea Criterion precasted gels (Bio-Rad) and transferred onto Hybond N+ membrane (Amersham Biosciences). Membranes were hybridized as previously describes [44] with oligonucleotide probes corresponding to the complementary sequences of the mature miRNAs: *miR-483-3p* 5'-UCACUCCUCUCCUCCCGUCUU-3' and the reference U6 RNA 5'-GCAGGGGCCATGCTAATCTTCTCTGTATCG-3'.

**Cell death and cell viability assays.** MTT assay was carried out on HEK293 cell line. HEK293 was cultured in 24-well plates the day before *miR-483-3p* or AMOs transfection. After 24 hours from transfection, cells were treated with doxorubicin (0.4 μg/ml) for additional 24 hours. The assay was performed in accordance with manufacturer's protocol (Sigma, TOX-1). Each experiment was performed in triplicate. Nuclear fluorescein staining based on labeling of DNA strand breaks by Terminal deoxynucleotidyl transferase (TUNEL-reaction) was performed on HepG2 cell line according to the manufacturer's instructions (In situ cell death detection kit, Cat. No.11684795910, Roche). The experiment was performed in triplicate and analyzed on microscope Zeiss Axiovert 200 at 100X magnification, images was acquire with the CCD Cascade Photometrics 512b. Quantification of positive nuclei was calculated by counting fluorescent spots in 10 images (10X10 magnifications) for each experiment. Caspase 3/7 activity assay was performed on HCT116 cell line. HCT116 was cultured in 96-well plates the day before miR-483-3p, AMOs and controls transfection. After 24 hours from transfection, cells were treated with Nutlin-3 (5 μM) or 5-Fluoruracil (from 0

to 50 μM) for additional 6/24 hours then the assay was performed in accordance with manufacturer's protocol (Promega, Caspase-Glo 3/7 assay, G8090).

**Generation of stable cell lines over-expressing miR-483-3p and antimiR-483-3p.** HCT116 cells were infected with the PMIRH483 expression plasmid containing the full-length miR-483-3p and the GFP gene under the control of two different promoters (PMIRH483PA-1, System Biosciences, Mountain View, CA). HCT116 and HepG2 cells were infected with the pSIH vector (System Biosciences, Mountain View, CA) containing the antisense sequence for miR-483-3p (**Table 1**) using the Lentivector-based Anti-MicroRNAs technology (miRZIP$^{TM}$, System Biosciences, Mountain View, CA). An empty vector was used as control. Pre-miR-483-3p, antimiR-483-3p expression and control constructs were packaged with pPACKH1 Lentivector Packaging Plasmid mix (System Biosciences) in 293-TN packaging cell line. Viruses were concentrated using PEG-*it*™ Virus Precipitation Solution and titers analyzed using UltraRapid Lentiviral Titer Kit (System Biosciences). Infected cells were selected by FACS analysis (FACS Calibur, Becton Dickinson Immunocytometry Systems). Infection efficiency >90% was verified by fluorescent microscopy.

***In vivo* studies.** Animal studies were approved by institutional ethical committee. HepG2 cells were transfected *in vitro* with 2'-O-methyl RNA oligonucleotide complemenmtary to miR-483-3p (anti-miR oligonucleotide: AMO-483-3p), AMO-Negative control from Fidelity Systems (Gaithersburg MD, USA) and siRNA against *IGF2* gene from Thermo-Scientific Dharmacon (Lafayette, CO, USA). At 24 h after the transfection, $10^7$ viable cells per mouse were injected intraperitoneally into ten Nod-Scid mice (Charles River Breeding Laboratories). After 35 days, the mice were sacrificed, necropsies were performed, and all tumors per mouse were weighed. For athymic "nude" mice experiments, HepG2 cells ($10 \times 10^6$ cells/200 ul) were injected subcutaneously into the flanks of nude mice 24 h after transfection with AMO-483-3p (4 injection), AMO Negative Control (4 injection) or siRNA IGF2 (6 injection). Tumors were counted after 20 days.

**Protein isolation, immunoblot analisis and immunoprecipitation.** Cells were collected from 6-well plates using trypsin-ethylenediaminetetraacetic acid (EDTA) (Sigma) and dissolved in lysis buffer (M-PER Mammalina Protein Extraction reagent, cat. 78501, Thermo Scientific) freshly supplemented with a complete protease inhibitor and phosphatase inhibitor cocktails 1 and 2 (Roche, Indianapolis, IN, USA) in accordance with manufacturer's

procedure. Nuclear extracts were prepared dissolving cells in nuclear and cytoplasmic extraction reagents (cat. 7833, Thermo Scientific) and following the manufacturer's procedure. After electrophoresis and blotting primary antibodies (Cell Signaling, anti-CTNNB1 #9562, anti-MYC #5605; Santa Cruz, anti-USF1 sc-229) were incubated over night at +4°C temperature and then peroxidase conjugated anti-mouse or anti-rabbit antibodies were incubated 1 hour at room temperature. Detection was conducted by chemiluminescent (Pierce ECL Western Blotting Substrate cat. 32106, Thermo Scientific). β-actin antibody (Cell Signaling, β-Actin Antibody #4967) or Vinculin antibody (Millipore, cat. MAB3574) were used to normalize protein loading. To quantify western blot signals, digital images of autoradiographies were acquired with Fluor-S MultiImager, and band signals were quantified in the linear range of the scanner using specific densitometric software (Quantity One). Immunoprecipitation was carried out with 100 µg of nuclear extracts in 500µl of binding buffer (10mM Tris, 50mM KCl, 1mM DTT; pH 7.5) with 2 µg of USF1 (Santa Cruz, sc-229) or CTNNB1 antibody (Cell Signaling, #9562) 2 hours at +4°C with gentle rotation. The immunoprecipitated was recovered by 25 µl of Protein A/G PLUS-Agarose (Santa Cruz, sc-2003) over night at +4°C with gentle rotation. Then the immunoprecipitated was washed in 0.1% NP40 three times and analyzed by western blot.

**Electrophoretic mobility shift assay (EMSA).** Protein/DNA binding was determined by electrophoretic mobility shift assay (EMSA) according to the manufacturer's procedure with biotinylated probes (Pierce, LightShift Chemiluminescent EMSA kit cat. 20148), see **Table 1** for oligo sequences. Samples were incubated with Ebox wt probe or the mutant form and with 100X Ebox wt unlabeled probe, and with specific polyclonal USF1 antibody (C-20, sc-229, Santa Cruz), before the addition of the probe. The DNA-protein complexes were resolved on 5% (w/v) nondenaturing acrylamide gels and visualized by exposure to autoradiographic films.

**Pull down experiment.** Pull-down assay was performed by using 10nmol of recombinant proteins GST (# ab85244, Abcam), GST-bcatenin (#ab63175, Abcam) and His-USF1 (#ab82069 Abcam). Reactions were carried out in binding buffer (150mM NaCl, 20mM Tris-HCl pH8, 1% NP40, 1mM EDTA), 1 mM PMSF and protease inhibitors at 4°C for 1 h of gentle rocking. The protein-protein complexes formed on the resin (Glutathione Sepharose 4 Fast Flow, Amersham or Ni-NTA Agarose, Qiagen) were brought down by centrifugation. The resin was washed five times for 5' at 4°C with 1 ml of cold wash buffer (250mM NaCl, 20mM Tris-HCl pH8, 1% NP40, 1mM EDTA). The protein complexes were resolved on

SDS-PAGE, immunoblotted and detection was conducted by chemiluminescent metti l'ECL (Pierce ECL Western Blotting Substrate cat. 32106, Thermo Scientific).

**DNA purification and Methylation analysis.** Genomic DNA was isolated from cell lines and tissue by standard treatment with sodium dodecyl sulfate and EDTA in the presence of 200 μg/ml of proteinase K, followed by phenol / chloroform extraction and ethanol precipitation. The methylation status of miR promoters was determined by Bisulfite Sequencing PCR (BSP) [45]. One microgram of genomic DNA was subjected to treatment with the EpiTect Bisulfite Kit (Qiagen) according to the manufacturer's instructions. Specific primers for PCR and sequencing were designed through the Methyl Primer Express v1.0 software (Applied Biosystems) (**Table 1).**

**Table 1.** Oligonucleotide sequences used for cloning, qRT-PCR, mutational analysis, site direct mutagenesis, bisulfate sequencing and EMSA assay.

| | *Gene* | *Name* | *Sequence* |
|---|---|---|---|
| **Gene Cloning** | CTNNB1 | CTNNB1_215F | ATGGCTACTCAAGCTGATTTGATGG |
| | CTNNB1 | CTNNB1_2560R | ACAGGTCAGTATCAAACCAGGC |
| | CTNNB1_3'UTR | bCAT_2677F_Xba | GttctagaTGCCACAAAAACAGGTAT |
| | CTNNB1_3'UTR | bCAT_3193R_Xba | GttctagaTTCAAAGCAAGCAAAGTC |
| | USF1 | USF1_BamHI_F | caaggatccCCCCCTCACAGAGAGATGAA |
| | USF1 | USF1_EcoRI_R | caagaattcGGATTAGGCTGTTGCTCCTG |
| | BBC3/PUMA | PUMA_3'UTR_F | GTGGACGTCAGGGACTCG |
| | BBC3/PUMA | PUMA_3'UTR_R | TTGAAAAGGAAACATACAAAAATCA |
| | miR-483 | MIRZIP_AS_miR-483-3p_U | CCGAGCTCGGGATCCTCACTCCTCTCCTCCCGTCTTCTTCCTGTCAGAAAGACGGGAGGAGAGGAGTGATTTTTGAATTCGCGGCCGC |
| | miR-483 | MIRZIP_AS_miR-483-3p_L | GGCGGCCGCGAATTCAAAAATCACTCCTCTCCTCCCGTCTTTCTGACAGGAAGAAGACGGGAGGAGAGGAGTGAGGATCCCGAGCTC |
| **qRT-PCRs (SYBR green)** | IGF2 | IGF2_3044F | TCCTCCCTGGACAATCAGAC |
| | IGF2 | IGF2_5965R | AGAAGCACCAGCATCGACTT |
| | IGF2 | IGF2_5965F | AAGTCGATGCTGGTGCTTCT |
| | IGF2 | IGF2_7866R | CGGAAACAGCACTCCTCAA |
| | IGF2 | IGF2_6907F | GTGAAATGGGCTCACAGGAT |
| | IGF2 | IGF2_7252R | AGCAATGCTCAGCTGGAAG |
| | IGF2 | IGF2_7846F | CGTTGAGGAGTGCTGTTTCC |
| | IGF2 | IGF2_8307R | GGACTGCTTCCAGGTGTCAT |
| | IGF2_3'UTR | IGF2-3 | CTTGGACTTTGAGTCAAATTGG |
| | IGF2_3'UTR | IGF2-2 | CGGGGATGCATAAAGTATGAG |
| | 18S | 18s_F | CTGCCCTATCAACTTTCGATGGTAG |
| | 18S | 18s_R | CCGTTTCTCAGGCTCCCTCTC |
| **qRT-PCRs ( Applied Taqman probe)** | IGF2-INS | Hs01005963_m1 | |
| | CTNNB1 | Hs00355045_m1 | |
| | MYC | Hs00153408_m1 | |
| | b-actin | Hs00357333_g1 | |
| | Pri-MiRNA hsa-mir-483 | Hs03293803_pri | |
| | hsa-miR-483-5p | Assay ID 002338 | |
| | hsa-miR-483-3p | Assay ID 002339 | |
| | RNU6B | Assay ID 001093 | |
| **Mutational analysis** | CTNNB1 | BCAT3 | AAAATCCAGCGTGGACAATGG |
| | CTNNB1 | BCAT2 | TGTTCTTGAGTGAAGGACTGA |
| | APC | APC_3361F | TTTTGGACAGCAGGAATGTG |
| | APC | APC_4091R | TGCTGGATTTGGTTCTAGGG |
| | APC | APC_4072F | CCCTAGAACCAAATCCAGCA |
| | APC | APC_4840R | TGTTGGCATGGCAGAAATAA |
| | Axin1 | Axin1_745F | CAGGCCACTATGGAGGAAAA |
| | Axin1 | Axin1_1583R | CTCTCAGGGTTCTCCTCGTG |
| | Axin1 | Axin1_1429F | ATGGAGGAGGAAGGTGAGGA |
| | Axin1 | Axin1_2186R | AGGGACAAGGGTCTGGAGTT |
| **Site direct mutagenesis** | miR-483 (promoter)_Ebox site | 483_Ebox-mut_F | CACCTGACACTCTTAGGTCTGGATCTTTACCACC |
| | miR-483 (promoter)_Ebox site | 483_Ebox-mut_R | GGTGGTAAAGATCCAGACCTAAGAGTGTCAGGTG |
| | CTNNB1 | CTNNB1_483mut_F | AACAATACAAATGGATTTTGTCGCCTCCTCAAGAAGTGAAGAATG |
| | CTNNB1 | CTNNB1_483mut_R | CATTCTTCACTTCTTGAGGAGGCGACAAAATCCATTTGTATTGTT |
| | miR-483 (promoter)_CTCF_BS1 | CTCF_mut1F | CTCCTGCTcactggCTGATaGCAtCTGCCCTTTGGC |
| | miR-483 (promoter)_CTCF_BS1 | CTCF_mut1R | cAGaTGCtATCAGccagtgAGCAGGAGCCCCATCAC |
| | miR-483 (promoter)_CTCF_BS2 | CTCF_mut2F | CCTTTGGCAAGGTGGAGCCCCCAGCGACCTTCCC |
| | miR-483 (promoter)_CTCF_BS2 | CTCF_mut2R | CCACCTTGCCAAAGGGCAGGTGCCATCAGCCGGA |
| | BBC3/PUMA | BBC3_mutF | AGGAGTCTGAATTAGGGGAGGGATGGCCCAG |
| | BBC3/PUMA | BBC3_mutR | CTCCCCTAATTCAGACTCCTCCCTCTTCCGAG |
| **Bisulfite Sequencing PCR** | miR-483 (promoter) | 483MetF2 | GGTAGGAAGTGGTATTGTAGGG |
| | miR-483 (promoter) | 483MetR2 | ACCCCCACAAAAAAAACTACT |
| **EMSA probes** | miR-483 (promoter) | 483_Ebox wt | ACCTGACACTCACCACGTGACATCTTTACCACC |
| | miR-483 (promoter) | 483_Ebox mut | ACCTGACACTCTTAGGTCTGGATCTTTACCACC |

## Results

***miR-483-3p* is over-expressed in Wilms' tumor and common adult human cancers in concert with IGF2.** Because of its location within the *IGF2* locus, I evaluated *miR-483-3p* expression in Wilms' tumor. Biopsies from 19 Wilms' tumors, four normal kidney tissues (three of which matched with Wilms' tumor samples), one fetal kidney and one fetal liver as positive control were analyzed. Up-regulation (from 4 to 40-fold) of miRNA expression was found in 73% of Wilms' tumors when compared with fetal kidney and in 100% of the cases when compared to non-tumoral kidney tissues (**Fig. 3A-B**). Northern blot analysis confirmed the qRT-PCR data (**Fig. 3C**).

Since *mir-483-3p* is located within the *IGF2* gene, I compared their levels of expression: a positive correlation between *IGF2* messenger RNA and *miR-483-3p* expression was found. By using two sets of primers spanning the junctions between exons 1-2 or 2-3 of the *IGF2* cDNA sequence I found strong positive coefficients of correlation with *miR-483-3p* in both cases ($R=0.94$, $p<0.0001$ for product E, and $R=0.60$, $p=0.004$ for product F) (**Fig. 3D**). These results indicate that the joint over-expression of at least two functional elements from the IGF2 locus, the IGF2 protein and *miR-483-3p*, may act in Wilms' tumors to promote tumorigenesis.

I investigated the potential involvement of *miR-483-3p* in common human neoplasms. I analyzed the expression of *miR-483-3p* in breast, colon and liver human cancers and I found that over-expression of *miR-483-3p* was indeed present, suggesting a wider involvement of this miRNA in human tumorigenesis. In primary colon, breast and liver carcinomas (**Fig. 4A-C**), I compared the expression of *miR-483-3p* of tumors with the average expression of non-tumor histological normal tissues. Considering the variability of *miR-483-3p* expression in non-tumor counterparts, only tumors exhibiting a fold-change > 10 in comparison with the average expression of non-tumor normal tissues were scored as over-expressed: 33% of HCCs, 31% of breast and 27% of colorectal cancers exhibited significant up-regulation. Interestingly, cirrhotic liver tissues, a condition that predisposes to HCC, already exhibited an increased miR-483-3p expression (from 3 to 14-fold) when compared to normal liver tissues (p-value < 0.05) (**Fig. 4A**).

I observed that, as in Wilms' tumors, the up-regulation of *miR-483-3p* was linked with *IGF2* expression: a positive Spearman coefficient of correlation of 0.69 for HCCs (p-value <0.0001) and 0.86 for CRCs (p-value <0.0001) (**Fig. 4A-B**).

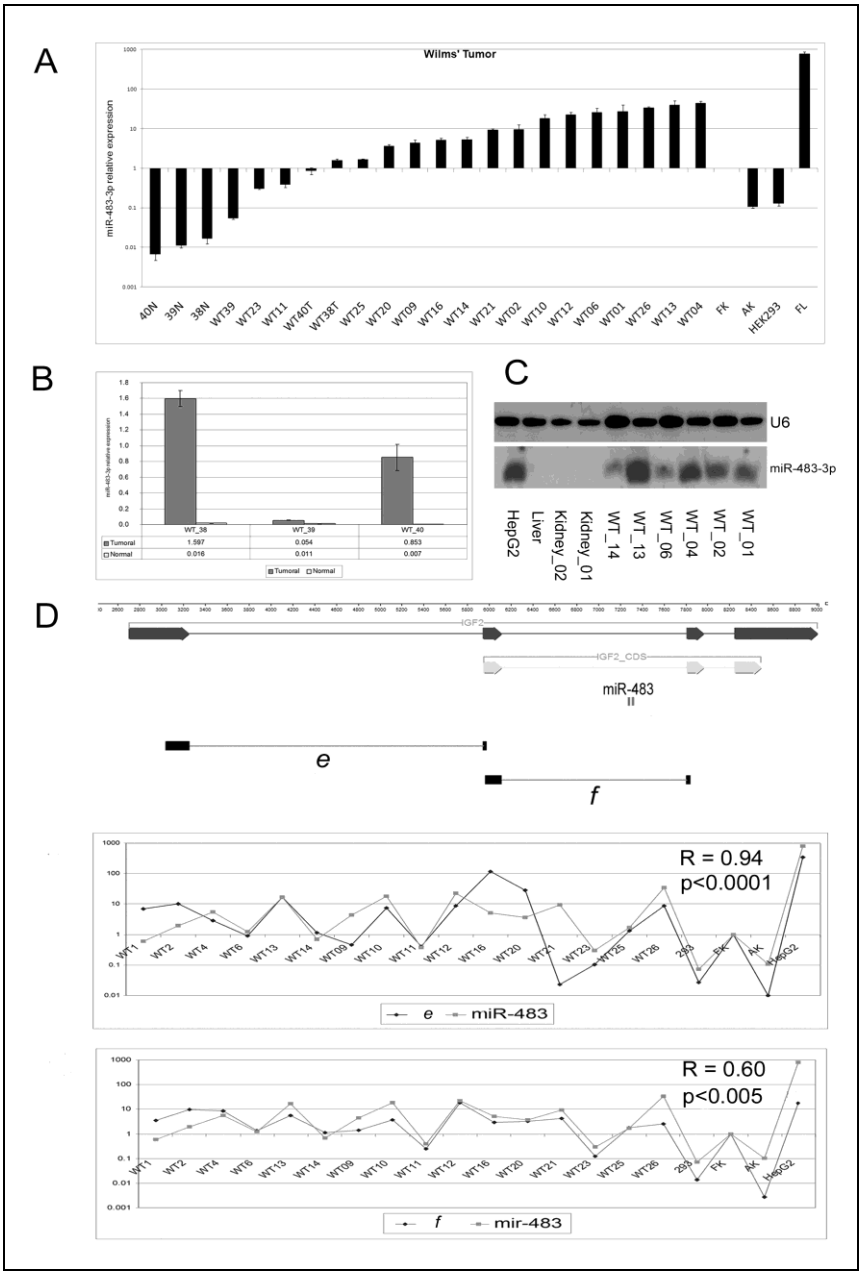


**Figure 3. miR-483-3p and IGF2 expression in Wilms' tumor**. (**A**) *miR-483-3p* relative expression analysis by quantitative real time PCR on 19 samples of primary Wilms' tumor, 3 adjacent non tumoral tissues, fetal kidney, cell line HEK293 and fetal liver tissue. Each sample data was normalized to the endogenous reference *RNU6B* and related to the Fetal Kidney (calibrator) miR-483-3p expression ($2^{-\Delta\Delta Ct}$ method). (B) Different expression from normal to tumoral tissue was pointed out in samples WT_38, _39 and _40. (C) Northern blot analysis of *miR-483-3p* and *RNU6B* in 6 Wilms' tumor samples, 2 normal adult kidney, 1 normal adult liver and HepG2 cell line. (D) Genomic structure of *IGF2* gene (black arrow); coding sequence is depicted as light gray arrows, miR-483 is indicated in the second *IGF2* intron. Black bars *e* and *f* show the cDNA amplified regions used to analyze *IGF2* expression that was compared to the *miR-483-3p* expression in panels immediately below. *IGF2* expression data were normalized on *RNA 18S* and related to *IGF2* fetal kidney expression ($2^{-\Delta\Delta Ct}$). Correlation coefficient (R) and the p-value (p) are shown.

In spite of these significant positive correlations, some tumor samples (HCC_02, HCC_04, HCC_10, HCC_13, HCC_16, HCC_21, HCC_26, HCC_29, CRC_188, CRC_130, CRC_148) exhibited a divergent expression of *IGF2* and *miR-483-3p*, suggesting the existence of multiple mechanisms of *miR-483-3p* regulation.

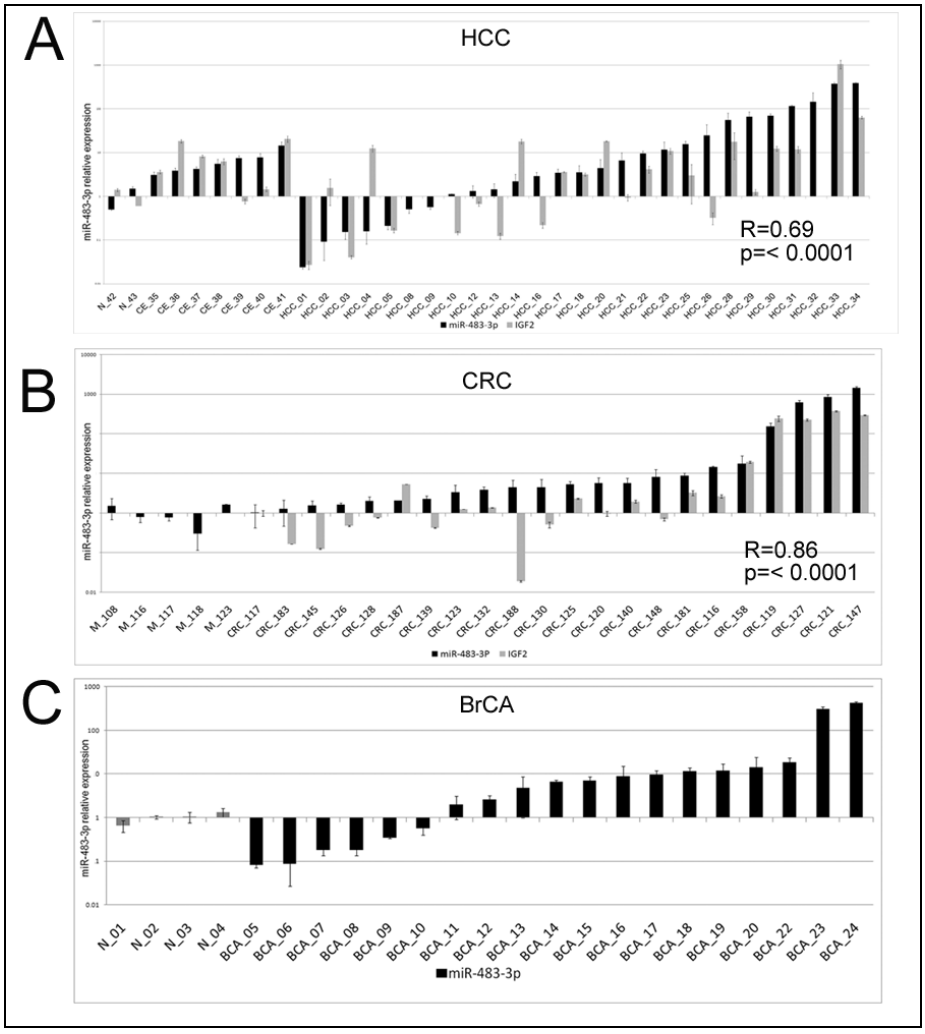


**Figure 4. miR-483-3p and IGF2 expression in adult human cancers.** *miR-483-3p* relative expression by quantitative real time RT-PCR. The expression of *miR-483-3p* was normalized to the endogenous gene *RNU6B* (black bars) while the expression of IGF2 was normalized in 18S RNA (gray bars). Expression data were related to the average expression of normal samples of each tissue ($2^{-\Delta\Delta Ct}$ method). Expression of the locus *IGF2/miR-483-3p* was investigated in (**A**) 27 HCCs and 7 non tumoral cirrhotic livers (CE), which were related to 2 normal liver tissue samples, the positive correlation between *IGF2* and *miR-483-3p* is indicated (R= 0.69, p<0.0001); (**B**) 22 colorectal cancer samples were related to 5 normal colon mucosa tissues, the positive correlation between *IGF2* and *miR-483-3p* is indicated (R= 0.86, p<0.0001); (**C**) 19 breast cancer and 4 normal breast tissues samples were tested for the expression of *miR-483-3p*.

**miR-483-3p protects cells from apoptosis**. To start unravelling the molecular basis of the potential oncogenic role of *miR-483-3p*, I focused on the apoptosis pathway because important pro-apoptotic human genes are predicted target by miRanda and TargetScan algorithms (*BBC3*/PUMA, *AMID*, *BAX*, *BIK*, *SMAC*/DIABLO, *PDCD1*, *PDCD7*). Thus, I evaluated apoptosis and cell viability in response to modulation of *miR-483-3p* in HEK293, HCT116 and HepG2 cells.

After treatment of HEK293 cells with doxorubicin to induce apoptotic cell death, transfection of *miR-483-3p* induced a low (10%) but significant increase in cell viability (p-value = 0.05), whereas transfection of anti-*miR-483-3p* AMOs induced a further 15% decrease in cell viability (p-value = 0.02) (**Fig. 5A**). These results indicate that *miR-483-3p* could promote cell survival.

HepG2 cells express very high level of *miR-483-3p*. Therefore, I evaluated only the effect of anti-*miR-483-3p* AMO in this cell line. Cell growth was 30 to 40% inhibited by transfection of anti-*miR-483-3p* AMO (**Fig. 5B**). Simultaneously, cells exhibited a 2.6 fold increase in the level of cell death than control cells transfected with a negative control AMO (p-value = 0.016) (**Fig. 5C**), as detected by *in situ* cell death using fluorescent labelling of DNA strand breaks with TdT (Terminal deoxynucleotidyl transferase).

To confirm that the mechanism was indeed apoptosis, caspase 3/7 activity was measured in HCT116 cells transfected with *miR-483-3p* or anti-*miR-483-3p* and treated with the apoptotic inducing factor Nutlin-3A. Compared to the controls, caspase activity exhibited an 80% increase in antimiR treated cells and a 60% decrease in *miR-483-3p* treated cells (**Fig. 5D**); moreover, I detected an inverse correlation between the amount of transfected miR-483-3p and caspase 3/7 activity, whereas a proportional increase was detected between AMO-483-3p and caspase 3/7 activity.

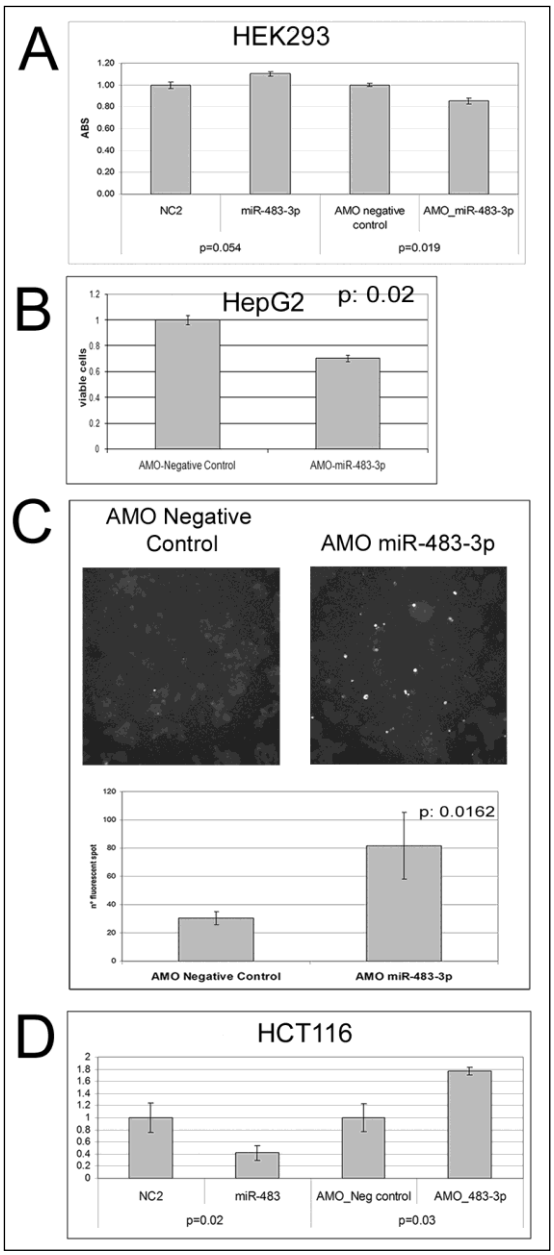


**Figure 5. AMO-483-3p induces cell death.** (**A**) Cell viability measured by the MTT assay in HEK293 cells. Each value represents the average absorbance ± standard deviation from three different experiments. The differences between miR-483-3p versus Negative Control 2 (p=0.002), and AMO_miR-483-3p versus AMO Negative Control (p=0.03) were both statistically significant. (**B**) Cell viability of HepG2 cells at 48 hours following transfection of AMO-miR-483-3p or AMO Negative Control. Each value represents average ± standard deviation from three different experiments (p=0.02 on AMO_miR-483-3p versus AMO Negative Control) and related to control data. (**C**) TUNEL staining of HepG2 cells after transfection of AMO-Negative Control or AMO miR-483-3p. Cells were stained 24 hours after transfection. Underneath the images, the average number of fluorescent spots is shown: data in each column represent the average ± standard deviation of fluorescent spots from three independent fields (p=0.0162). (**D**) Caspase 3/7 activity in HCT116 cells transfected with miR-483-3p, anti-miR-483-3p AMO or Negative controls; after 24 hours, cells were treated with Nutlin-3 (5μM) for additional 6 hours.

**PUMA is targets of miR-483-3p.** In the list of potential pro-apoptotic target genes, BBC3/PUMA (BCL2 binding component 3 / p53 upregulated modulator of apoptosis) gene was chosen for further analysis because of its known pivotal role in induced cell death [46].

To test the direct interaction of *miR-483-3p* with 3'UTRs, the predicted wild type and mutant *miR-483-3p* target sites of PUMA mRNA gene was cloned downstream of the luciferase reporter gene of pGL3-Control vector. The HEK293 cells were used as biological system because they exhibit a low expression of *miR-483-3p*, HCT116 cells have a medium expression whereas the HepG2 cells exhibit a high expression of miR-*483-3p* (**Fig. 6**).

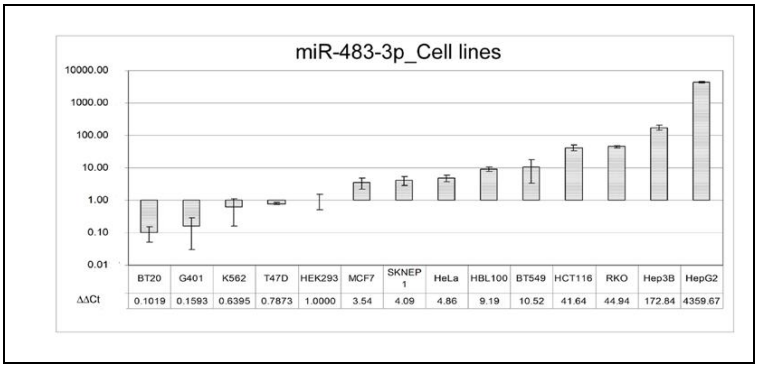


**Figure 6.** *miR-483-3p* relative expression analysis by quantitative real time PCR on 14 cell lines. Each sample data was normalized on the *RNU6B* (ΔCt method) and related to the HEK293 *miR-483-3p* expression (ΔΔCt method).

Dependently the *miR-483-3p* expression the *miR-483-3p* responsive vector was co-transfected with *miR-483-3p* into HEK293, either miR-*483-3p* or anti*miR-483-3p* oligonucleotide (anti-483-3p AMO) into HCT116 cells and only anti*miR-483-3p* into HepG2 cells (**Fig. 7A**). In comparison with control vector, *miR-483-3p* induced a decrease in luciferase activity of about 38% (HEK293) and 45% (HCT116) of the pGL3 vector carrying the PUMA-3'UTR, whereas in the mutated 3'UTR clone the luciferase activity was not significantly down-regulated by *miR-483-3p*. Conversely, the use of anti-*miR-483-3p* AMOs induced an increase in luciferase activity of about 70% and 39% for HCT116 and HepG2 cells, respectively (**Fig. 7B**).

To further confirm PUMA as target of *miR-483-3p*, its protein level was assessed by western blot analysis on HEK293 and HepG2 cells transfected with *miR-483-3p* or anti*miR-483-3p* respectively. Protein expression was reduced (70%) in HEK293 and induced (40%) in HepG2 cells when compared to the controls (**Fig. 7C**).

The analysis of two matched Wilms' tumors / normal kidney samples for the expression of PUMA protein revealed that, as predicted by the molecular function of *miR-483-3p*, the level of expression of these two pro-apoptotic proteins was significantly lower in tumors, where *miR-483-3p* is expressed at higher level (**Fig. 7D**).

To further support these data I generated stable cell lines over-expressing the *miR-483-3p* or the anti*miR-483-3p* to evaluate the expression of BBC3/PUMA after treatment with 5-Fluorouracil (5FU) as an apoptosis inductor factor that involve the P53 pathway. The HCT116

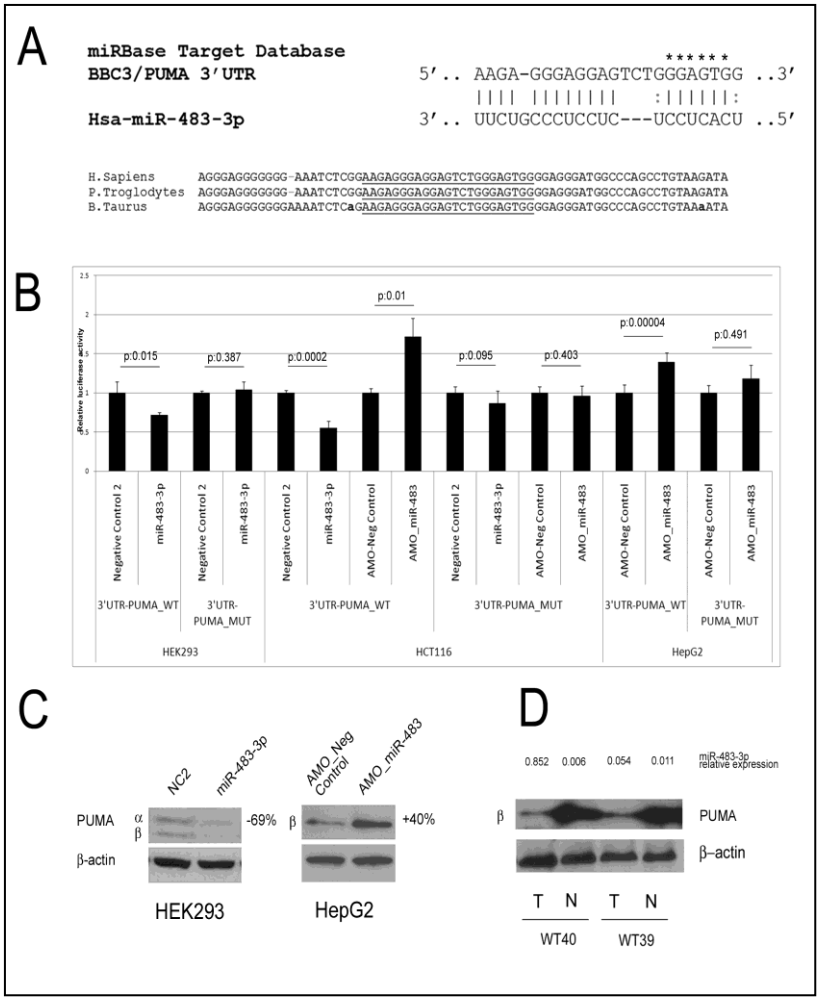


**Figure 7. BBC3/PUMA is target of miR-483-3p.** (**A**) Putative binding site of *miR-483-3p* in PUMA 3'UTRs (miRBase Target Database). Asterisks show nucleotides substituted in miR-483-3p predicted target site to perform luciferase assay (GGAGT>AATTA). (**B**) PUMA 3'UTRs regulates luciferase activity dependent on *miR-483-3p* in HEK293, HCT116 and HepG2 cell lines (WT, wild type; MUT, mutant; p, p-value). Firefly luciferase activity was normalized on Renilla luciferase activity of the cotransfected pRL-TK vector. (**C**) Western blot analysis of PUMA after *miR-483-3p* transfection in HEK293 and HepG2 cell line, the α (23 KDa) and β (18 KDa) isoforms are indicated. Cells were collected after 48 hours after miRNA transfection. (**D**) Western blot analysis of PUMA in Wilms' tumor samples (T) and matched normal tissues (N).

cells were infected with lentiviral vectors over-expressing *miR-483-3p* (LV-483) or anti*miR-483-3p* (LV-AS483), whereas the HepG2 cell line was infected with LV-AS483. An empty vector as control was used (LV-CTRL). The increased concentrations of 5FU match with the increased PUMA protein levels only in the HCT116 and HepG2 cells over-expressing the anti*miR-483-3p* **(Fig. 8A),** in spite of a homogeneous increment of BBC3/PUMA mRNA levels **(Fig. 9A)** in all stable cell lines. The induction of both BBC3/PUMA and CDKN1A/p21 mRNA levels by 5FU treatment suggest the activation of P53 pathway (**Fig. 9A-B**).

To assess the physiologic role of this finding, the caspase 3/7 activity of these stable cell lines was measured after 5FU treatment. Compared to controls the HCT116-LV-483 cells showed a reduced caspase 3/7 activity (24- 40%, $p<0.0001$) **(Fig. 8B)** whereas the HCT116-LV-AS483 exhibited an increased activity (4 to 28%, p: 0.03). As expected also in HepG2-LV-AS483 cells the caspase activity was increased (21 to 70%, $p<0.0001$) **(Fig. 8B)**. To further prove the connection between *miR-483-3p*, PUMA and apoptosis, I proved that by knocking

down PUMA by siRNA transfection, I could prevent the AS483-3p effect in HepG2-LV-AS483 cells (**Fig. 8C)**. I used the HepG2 stable cell lines because the efficacy of the anti-miR-483-3p is more evident than the HCT116 model **(Fig.8B)**.

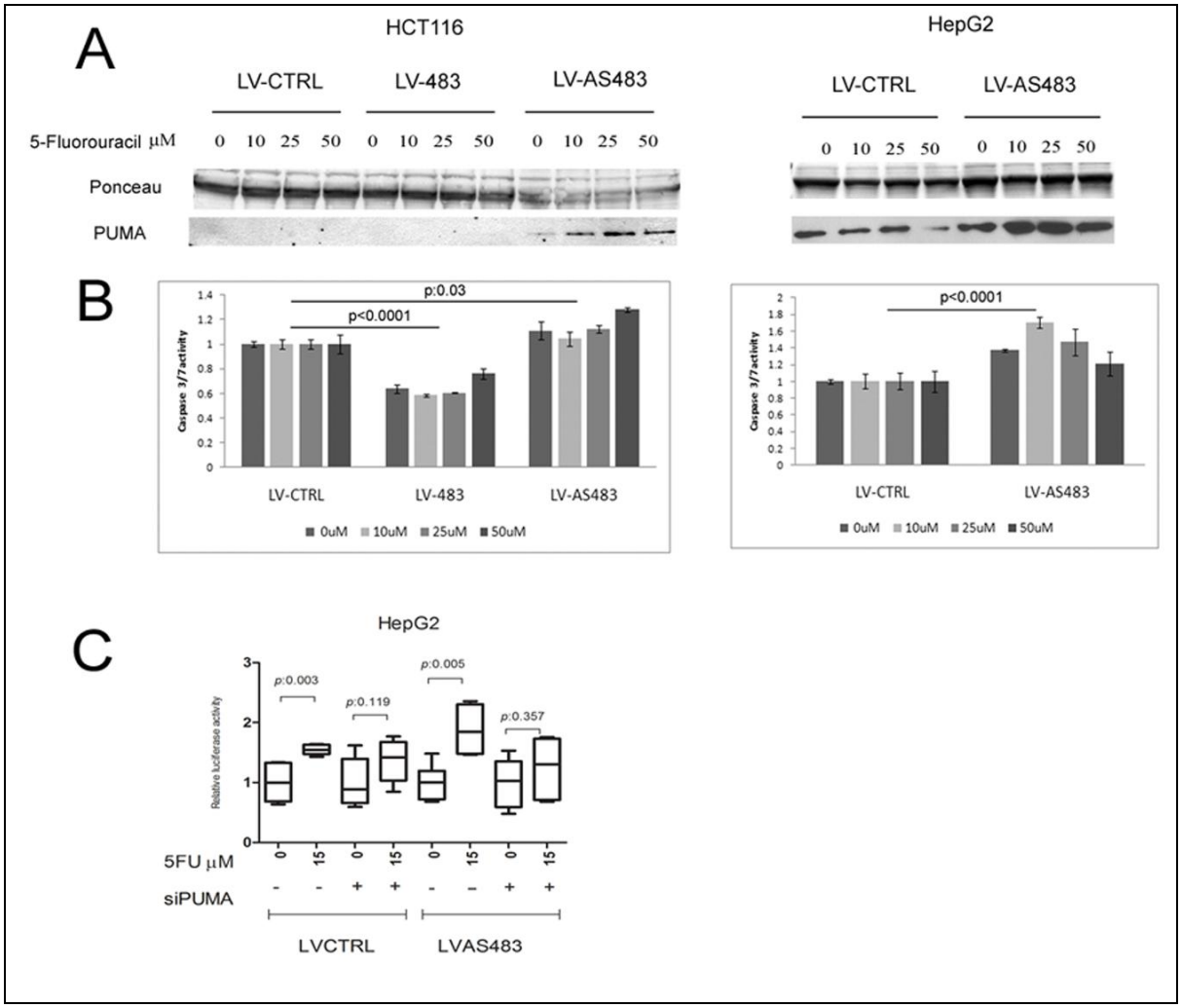


**Figure 8. Stable cell lines over-expressing antimiR-483-3p are more sensitive to apoptosis stimuli.** HCT116 cells over-expressing the miR-483-3p (LV-483) or the antimiR-483-3p (LV-AS483) and HepG2 cells over-expressing the antimiR-483-3p were treated with different concentration of 5-Fluorouracil. LV-CTRL indicates stable cell line with the empty vector. **(A)** Western blot analysis reveals an increment of PUMA protein levels only in the cells LV-AS483. **(B)** Caspase 3/7 activity was decreased in LV-483 cells and increased in LV-AS483 when compared with LV-CTRL cells. Data were normalized on LV-CTRL cells. **(C)** Relative caspase 3/7 activity in HepG2-LV-CTRL and LV-AS483 after treatment with 5FU and siPUMA (+) or siRNA scramble (-).Data were normalized on average of caspase activity of HepG2-LV-CTRL cells.

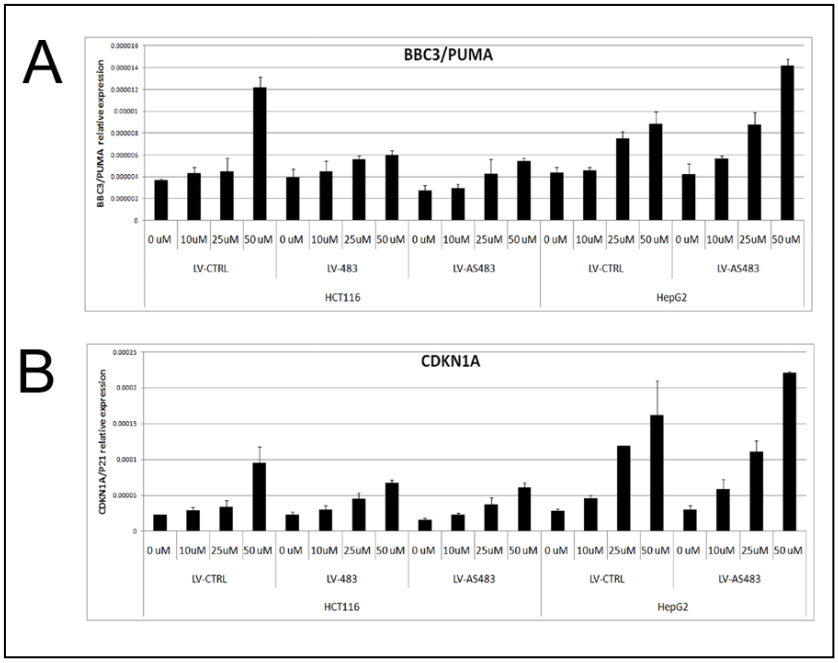


**Figure 9 CDKN1A/P21 RNA induction in stable cell lines after 5-Fluorouracil treatment.** qRT-PCR analysis of CDKN1A/P21 expression was normalized on 18S RNA.

**AMO-miR-483-3p but not IGF2 siRNA can inhibit *in vivo* tumorigenicity.** The potential oncogenic role of *miR-483-3p* was directly tested through tumorigenicity modulation of the human HepG2 cells, which over-expresses miR-483-3p. Twenty-four hours after transfection of AMO-483-3p or siRNA anti-IGF2 into HepG2 cells, a qRT-PCR confirmed the specific reduction of *miR-483-3p* or *IGF2* mRNA, respectively **(Fig. 10A)**. Then, $10\times10^6$ cells (cell viability greater than 97%) were intra-peritoneally injected into Nod-Scid mice. Mice were sacrificed on day 35 and all tumors for each mouse weighed. AMO-483-3p mouse group showed a significant reduction of number and weight of induced tumors compared to controls (p-value <0.05). On the contrary, repression of the *IGF2* gene did not show any difference from controls (p-value >0.5) **(Fig. 10B-C)**. The three groups of data (CTRL, AMO-483-3p, siIGF2) are comparable because of the same nature of the molecules used to silence the *miR-483-3p* and *IGF2* gene (2'-O-methyl RNA oligonucleotide).

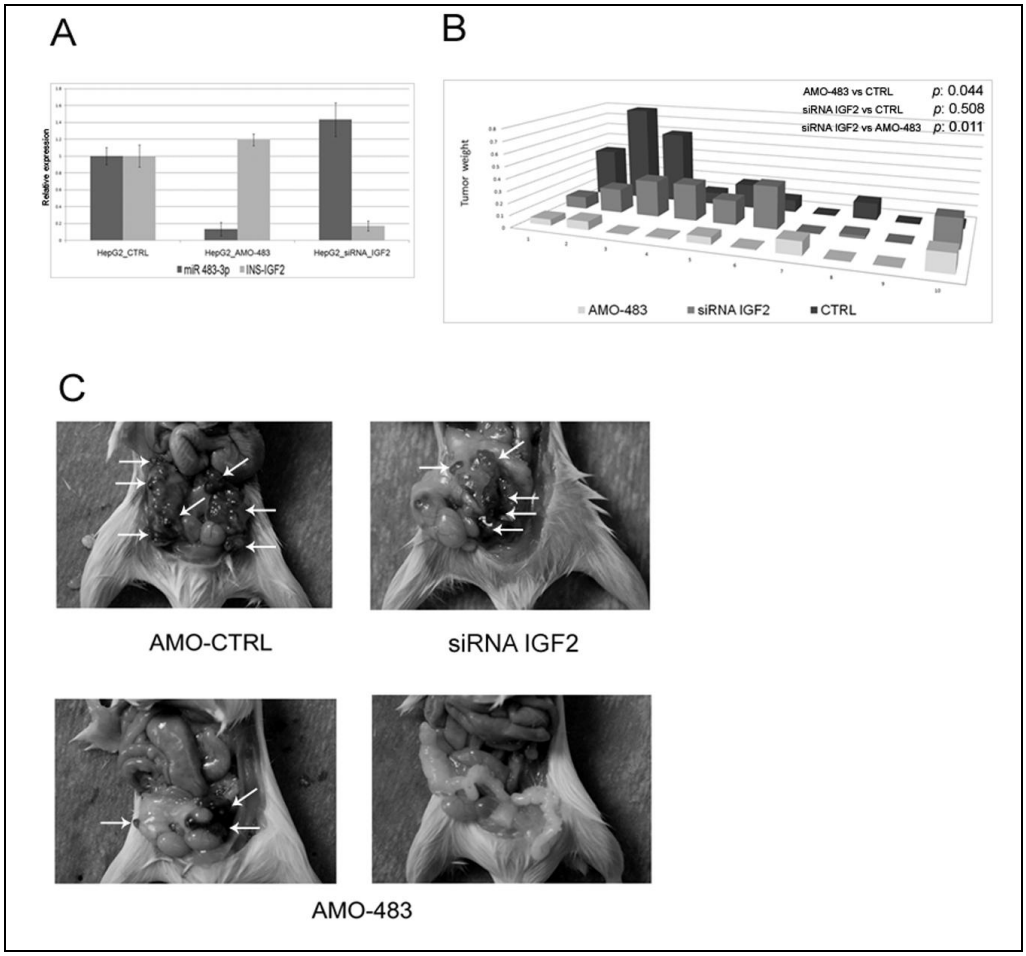


**Figure 10. AMO-483-3p reduces tumors induced by HepG2 cells *in vivo*. (A)** A qRT-PCR analysis to verify reduction of *miR-483-3p* and *IGF2* mRNA after transfection of AMO-483-3p or siRNA anti-IGF2 in HepG2 cells. **(B)** Tumors of each mouse were weighed: a significant difference ($p<0.05$) in tumor weights was found between AMO-483-3p and AMO Negative control transfected (CTRL) cells, between siRNA IGF2 and AMO-483-3p ($p<0.02$) but not between siRNA IGF2 and AMO-CTRL transfected HepG2 cells ($p>0.5$). **(C)** Appearance of intraperitoneal HepG2 induced tumors in Nod-Scid mice: the white arrows indicate tumor formations.

**miR-483-3p expression correlates with the mutational status of Wnt/β-catenin genes in hepatocarcinoma (HCC).** The Wnt/β-catenin pathway is one of the most important pathways dysregulated in hepatocarcinoma (HCC), colorectal cancer (CRC) and Wilms' tumor [47-49]. Since I previously found that *miR-483-3p* is up regulated in these cancers as well, I investigated the possible involvement of Wnt/β-catenin in *miR-483-3p* dysregulation. Since *miR-483-3p* is located within intron 2 of the *IGF2* gene I previously found a positive correlation between *IGF2* and *miR-483-3p* expression in HCC ($R=0.69$, $p<0.0001$), CRC tumor samples from HCC that have a low coefficient of correlation, exhibited a divergent expression of *IGF2* and

**Table 2. Mutational status of Wnt/β-catenin genes is associated to miR-483-3p expression.** 24 HCC samples analyzed for IGF2, miR-483-3p expression and for the mutational status of CTNNB1 exon 3, APC and Axin genes.

| *Sample* | *miR-483-3p relative expression* | *IGF2 relative expression* | *Ratio 483/IGF2* | *CTNNB1 ex 3 status* | *APC status (NM000038 from nt 3361 to 4840)* | *Axin 1 status (NM003502 from nt 745 to 2186)* |
|---|---|---|---|---|---|---|
| **HCC_01** | 0.02 | 0.03 | 0.9 | 0 | 0 | 0 |
| **HCC_02** | 0.09 | 1.55 | 0.1 | **GAC->TAC_Asp32->Tyr** | 0 | NC |
| **HCC_03** | 0.15 | 0.04 | 3.8 | 0 | 0 | 0 |
| **HCC_04** | 0.16 | 12.47 | 0.0 | 0 | 0 | 0 |
| **HCC_05** | 0.21 | 0.17 | 1.3 | 0 | NC | NC |
| **HCC_10** | 1.12 | 0.14 | **7.7**** | 0 | 0 | NC |
| **HCC_12** | 1.32 | 0.67 | 2.0 | NC | 0 | NC |
| **HCC_13** | 1.44 | 0.12 | **11.7**** | 0 | 0 | 0 |
| **HCC_14** | 2.20 | 17.90 | 0.1 | 0 | 0 | 0 |
| **HCC_16** | 2.92 | 0.22 | **13.3*** | 0 | 0 | NC |
| **HCC_17** | 3.47 | 3.58 | 1.0 | 0 | 0 | 0 |
| **HCC_18** | 3.54 | 3.18 | 1.1 | 0 | 0 | 0 |
| **HCC_20** | 4.47 | 18.02 | 0.2 | NC | NC | NC |
| **HCC_21** | 6.63 | 0.94 | **7.0**** | 0 | **del 3719-3740** | 0 |
| **HCC_22** | 9.55 | 4.15 | 2.3 | 0 | 0 | 0 |
| **HCC_23** | **11.63*** | 10.89 | 1.1 | **TCT->CCT_Ser37->Pro** | 0 | 0 |
| **HCC_25** | **15.73*** | 3.01 | **5.2**** | **TCT->TAT_Ser37->Tyr** | 0 | 0 |
| **HCC_26** | **24.98*** | 0.32 | **77.1**** | **CAT->CCT_His36->Pro** | 0 | 0 |
| **HCC_28** | **55.52*** | 17.62 | 3.2 | 0 | 0 | 0 |
| **HCC_29** | **66.03*** | 1.26 | **52.3**** | 0 | 0 | **del 1024-1027nt** |
| **HCC_30** | **69.23*** | 12.29 | **5.6**** | **GAC->GGC_Asp32->Gly** | 0 | 0 |
| **HCC_31** | **116.16*** | 11.78 | **9.9**** | 0 | 0 | 0 |
| **HCC_33** | **374.10*** | 1050.30 | 0.4 | 0 | 0 | NC |
| **HCC_34** | **388.40*** | 63.37 | **6.1**** | 0 | NC | **CCT->ACT_Pro486->Thr** |

NC; not classified
0; not mutated
* miR-483-3p expression values greater than the considered cut-off (10)
**miR-483-3p/IGF2 expression ratio values greater than the considered cut-off (5)

*miR-483-3p* suggesting alternative mechanisms regulating these two genes. I analyzed the mutational status of *APC*, *CTNNB1* and *Axin1* in 24 HCC samples in which *miR-483-3p* and *IGF2* expression had already been assessed [40]. Mutations in these three genes were previously proposed as a major cause of activation of the Wnt/β-catenin pathway in cancer [50 51 28]. With a *miR-483-3p* expression cut-off level of 10-fold over the average expression of the controls, I detected an association between *miR-483-3p* up regulation and mutational status of these genes (p=0.053; Fisher's Exact Test) (**Tab. 2**), whereas no association between *IGF2* expression and the Wnt/β-catenin mutational status was found (expression cut off = 10, p > 0.5; Fisher's Exact Test). These data suggest that β-catenin may be involved in the regulation of *miR-483-3p* separately from *IGF2*. To prove this point I calculated the ratio between *miR-483-3p* and *IGF2* expression levels (median value =1.3) to identify samples in which they were divergent (**Tab. 2**). A strong association between the miR-483-3p/IGF2 ratio and the mutational status of the Wnt/β-catenin genes was observed when the ratio is greater than 5 (p=0.015; Fisher's Exact Test). Overall these data strongly suggest that expression of *miR-483-3p*, but not that of *IGF2*, is associated with the mutational status of the Wnt/β-catenin pathway.

**The miR-483 locus is regulated by β-catenin.** Since β-catenin is the principal transcriptional mediator of the Wnt/β-catenin pathway, I investigated its involvement in the regulation of the *IGF2*/*miR-483* locus. I cloned the coding sequence of the β-catenin gene into the expression vector pIRES-Neo2, and tested its expression (**Fig 11A** top panel) and ability to activate the luciferase reporter vector pGL3-OT containing the β-catenin/TCF responsive element (**Fig.S1)** [52]. pGL3-OF, which carries a mutated β-catenin/TCF binding site, was used as a negative control. Then I assessed the expression level of *miR-483-3p* in response to β-catenin over-expression in HEK 293 cells. A significant increase in *miR-483-3p* expression was detected in cells transfected with pIRES-Neo2-βcatenin vector compared to cells transfected with the empty vector pIRES-Neo2 (**Fig. 11A**). To confirm these results, I transiently knocked-down β-catenin by using short interfering RNA technology (siRNA) in HCT116 cells that exhibits a higher β–catenin nuclear activity, and miR-483-3p expression, compared to HEK293 cells. qRT-PCR verified the decrease of β-catenin mRNA after siRNA treatment (**Fig.S1B)**, and a significant reduction of *miR-483-3p* expression was detected only in cells transfected with β-catenin siRNA (**Fig.12B)**.

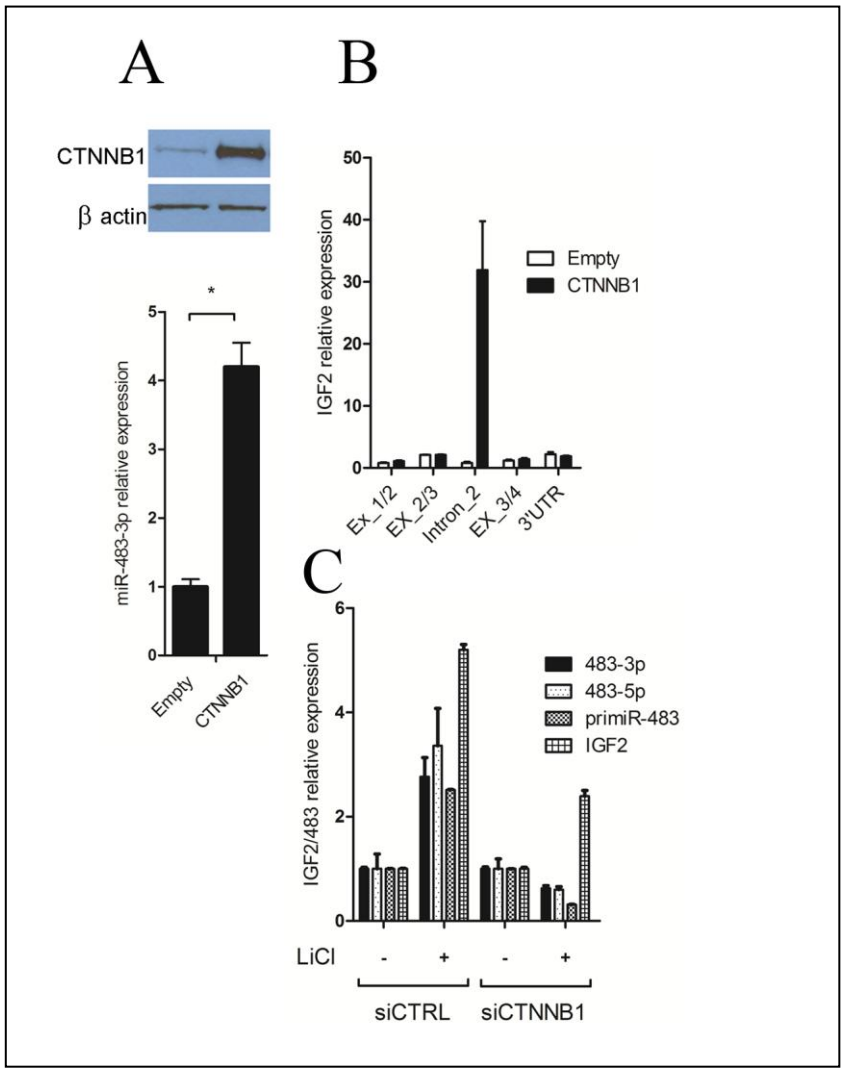


**Figure 11. Induction of miR-483-3p expression by β-catenin.** (**A**) *miR-483-3p* was induced by enforced expression of *CTNNB1* wild type. Expression value was related to the miRNA expression on empty vector transfected cells ($2^{-\Delta\Delta Ct}$).The expression of CTNNB1 was assessed by western blot (top panel). (**B**) Expression analyses across the *IGF2* locus modulated by the enforced expression of β-catenin. Three PCR products were designed to amplify *IGF2* exon junctions (Ex_1/2, Ex_2/3, Ex_3/4) and one its 3'UTR (3'UTR). One set of primers was located within intron 2 and was used to assess the expression of miR-483 precursor (intron_2). qRT-PCRs were carried out with SYBR green technologies. RNA was previously treated with DNAse to avoid genomic contamination. Black bars show the expression detected in cells transfected with the *CTNNB1* expressing vector; white bars show the expression detected in cells transfected with the Empty vector. (**C**) Expression analysis of the miR-483-3p, miR-483-5p, primiR-483 and IGF2 genes assayed by qRT-PCR using TaqMan probes after LiCl treatment (20mM for 24hours) with and without siRNA for CTNNB1 gene. *IGF2* expression was still induced, although more weakly than the control (**Fig 11C)**. This *IGF2* induction by LiCl has not been previously described and is not necessarily due to β-catenin because of the large number of pathways affected by GSK3B inihibition. Single asterisk indicates a p value<0.02.

Next I investigated the effect of β-catenin on *IGF2* expression. By real time PCR (RT-qPCR) I evaluated the expression of different DNA segments across the *IGF2* gene locus using 5 sets of primers spanning the junctions between the *IGF2* cDNA sequence and the *IGF2* intron 2. The only DNA segment whose transcription was induced by β-catenin was within the second intron of the *IGF2* that includes *miR-483-3p* (**Fig 11B**). Thus I concluded that β-catenin activates a *miR-483-3p* promoter inside the second intron of *IGF2*.

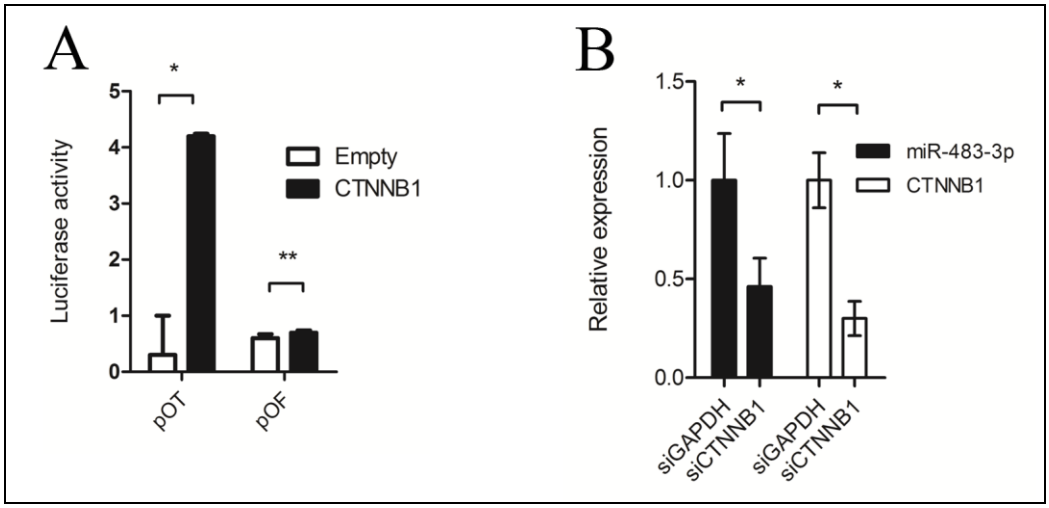


**Figure 12.** (**A**) Ability to activate the luciferase reporter vector pGL3-OT containing the b-catenin/TCF responsive element by exogenous expression of b-catenin. pGL3-OF, which carries a mutated b-catenin/TCF binding site, was used as a negative control. (**B**) *miR-483-3p* (white bars) and *CTNNB1* (black bars) relative expression in HCT116 cell line transfected with *CTNNB1* and *GAPDH* siRNAs at 36 hours from transfection

To further confirm these results, I stabilized β-catenin protein by treating HEK293 cells with lithium chloride (LiCl), an inhibitor of GSK3B which is responsible for β-catenin degradation. **Figure 11** shows that expression of the entire IGF2/miR-483 locus (*miR-483-3p, 5p, pri-miR-483* and *IGF2*) was significantly activated (3 to 5 fold) by LiCl treatment. Conversely, treatment with β-catenin siRNA resulted in reduced expression of the *miR-483* locus after LiCl treatment. *IGF2* expression was still induced, although more weakly than the control (**Fig 11C)**. This *IGF2* induction by LiCl has not been previously described and is not necessarily due to β-catenin because of the large number of pathways affected by GSK3B inihibition. Taken together, these results suggest that the *miR-483* locus expression can be driven by β-catenin independently from *IGF2*.

**The zinc finger CCCTC-binding factor CTCF represses the genomic region upstream of the miR-483 locus.** To explore the connection between β-catenin and expression of the *miR-483* locus I cloned 4 fragments of different length including the putative *miR-483* promoter (**Fig 13A**) upstream of the luciferase gene into the pGL4 enhancer vector (pGL4E). **Figure 13B** shows LiCl treatment causes significant induction of luciferase activity for all fragments except the small clone pGL4E-6907 (**Fig 13B**).

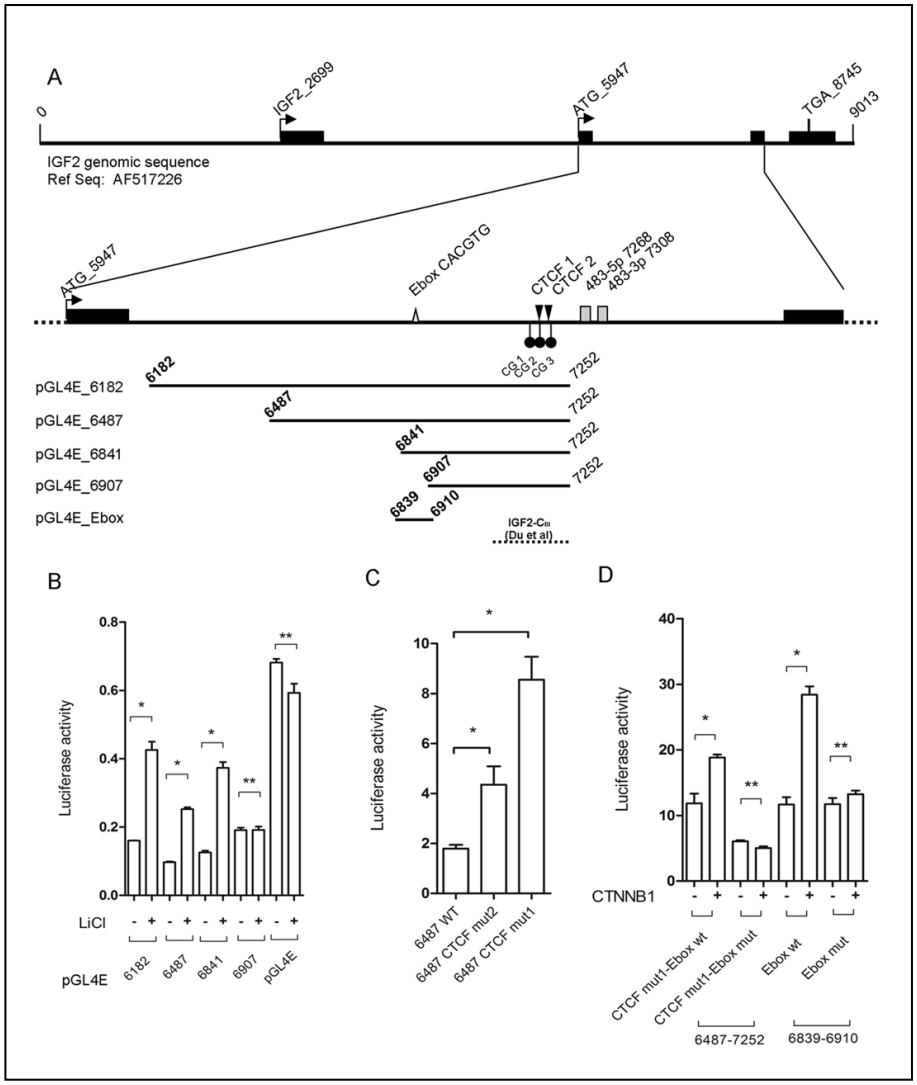


**Figure 13. Analysis of the miR-483 minimal promoter region responsive to LiCl/CTNNB1 stimuli.** (**A**) Genomic structure of IGF2/483 locus from the reference AF517226 genomic sequence. Exons (black bars), start (ATG_5947) and stop codon (TGA_8745), the Ebox elements (gray triangle), the two predicted CTCF binding sites (black triangle), three CpG dinucletides around the CTCF binding sites (black circles), miR-483-3p and miR-483-5p (gray boxes) are shown. Are indicated the 5 genomic fragments cloned upstream the luciferase reporter gene in pGL4E for the analysis of the promoter on the bottom of the panel. The genomic region with insulator activity studied by Du et al. is indicated (broken line). (**B**) Luciferase activity of 4 genomic fragments cloned in pGL4E with and without LiCl treatment, the pGL4E empty vector was used as control. (**C**) Luciferase activity of the pGL4E_6487 wild type (WT) and the pGL4E_6487 mutated in the predicted CTCF binding sites (CTCFmut1and CTCFmut2). (**D**) Analysis of the Ebox element wild type (Ebox wt) and mutant (Ebox mut) by luciferase assay on the pGL4E_6487 CTCF mut1 and pGL4E_Ebox. Firefly luciferase activity was normalized on Renilla luciferase activity of the cotransfected pGL4R vector. Single asterisk indicates a p value<0.02, double asterisk indicates a p value>0.02.

Thus I inferred that the genomic region responsive to LiCl treatment is located between positions 6841 and 6907 of the reference sequence AF517226.

Because the luciferase activity in each of these vectors with or without LiCl treatment was always lower than the control (pGL4E empty vector), I suspected the presence of a repressive element within this region. Du et al. has shown that a 151 bp fragment (called IGF2-$C_{BI}$ by the authors, **Fig 13A**), immediately upstream of the miR-483 stem loop, has strong insulator activity and binds to the CTCF repressor [53]. CTCF is an important methyl sensitive regulator of transcription involved in the epigenetic regulation of genomic imprinted loci such as the IGF2/H19 locus in 11p15.5.

**Table 3.** Methylation status of the 3 CpG dinucleotides close to the CTCF binding site

| *Cell line* | *miR-483-3p relative expression* | *Methylation status CpG 1 (%)* | *Methylation status CpG 2 (%)* | *Methylation status CpG 3 (%)* |
|---|---|---|---|---|
| **H460** | 0.015 | 0 | 50 | 0 |
| **SNU 423** | 0.022 | 0 | 50 | 0 |
| **PLC/PRF/5** | 0.029 | 0 | 0 | 0 |
| **SNU 449** | 0.042 | 0 | 50 | 50 |
| **MDA MB231** | 0.23 | 75 | 100 | 50 |
| **K562** | 0.639 | 25 | 50 | nc |
| **SW 480** | 0.697 | 0 | 0 | nc |
| **SNU 387** | 0.759 | 25 | 50 | nc |
| **SKHEP 1** | 0.789 | 0 | 0 | 0 |
| **HEK293** | 1 | 50 | 100 | 100 |
| **MCF7** | 3.543 | 75 | 100 | 100 |
| **HEPG2** | 23.87 | 100 | 100 | 100 |
| **HUH 7** | 44.985 | 100 | 100 | 100 |
| **HEPG2-C3A** | 51.464 | 75 | 100 | 100 |

CTCF binds DNA elements called insulators which set limits on the action of enhancer or silencer elements permitting to the genome to be organized in functional regulatory domains [54]. It is involved in Wilms' tumor [16 55 56], breast cancer [57 58] and prostate cancer [59]. I decided to determine if CTCF is also involved in the repression of the *IGF2/mir-483* genomic regions I cloned. Using bioinformatics tools (http://insulatordb.uthsc.edu) I identified two possible CTCF binding sites (CTCF BS_1, CTCF BS_2) (**Fig 13A**). By transfecting the pGL4 vectors with mutated versions of either CTCF BS_2 or CTCF BS_1 to prevent CTCF binding, I observed a 2 or 4 fold increase of the luciferase activity compared to the wild type control (**Fig 13C**). Since the CTCF repressor only binds demethylated DNA, I analyzed the methylation status of 3 CpG dinucleotides close to the CTCF binding sites in a set of 14 cell lines. I found a significant positive correlation between the methylation level of the first CpG (CG_1, **Fig 13A**) and *miR-483-3p* expression (R=0.682, p=0.007), whereas the correlation with each of the other 2 CpGs was less significant (**Tab 3**). These data indicate that CTCF is an important regulator of the *miR-483* locus and this regulation is likely affected by DNA methylation.

**The transcription factor USF1 serves as a mediator between β-catenin and the miR-483 locus.** The minimal genomic region responsive to LiCl treatment (between nucleotides 6841 and 6907) contains an E-box motif (CACGTG) that could bind the basic Helix-Loop-Helix (bHLH) protein family. One of these bHLH proteins is the MYC transcription factor, a well known target of the Wnt/β-catenin pathway, therefore it is reasonable to speculate that MYC

could be involved in the LiCl regulation of the *miR-483* locus. To test this hypothesis, I mutated the pGL4E-6487 in the E-box site and also mutated CTCF BS_1 to partially eliminate the repressive activity of this region. After co-transfection of β-catenin and the reporter vectors into HEK293 cells there was a significant induction of luciferase activity in the wild type but not in the E-box mutant clone (**Fig 13D**). This confirmed the data obtained after LiCl treatment (**Fig 13B**) and identified within the E-box motif the sequence responsive to the β-catenin/LiCl stimulation. Similar results were obtained with the vector clone containing only 69 base pairs around the E-box motif (pGL4E-6841-6910) (**Fig 13D**).

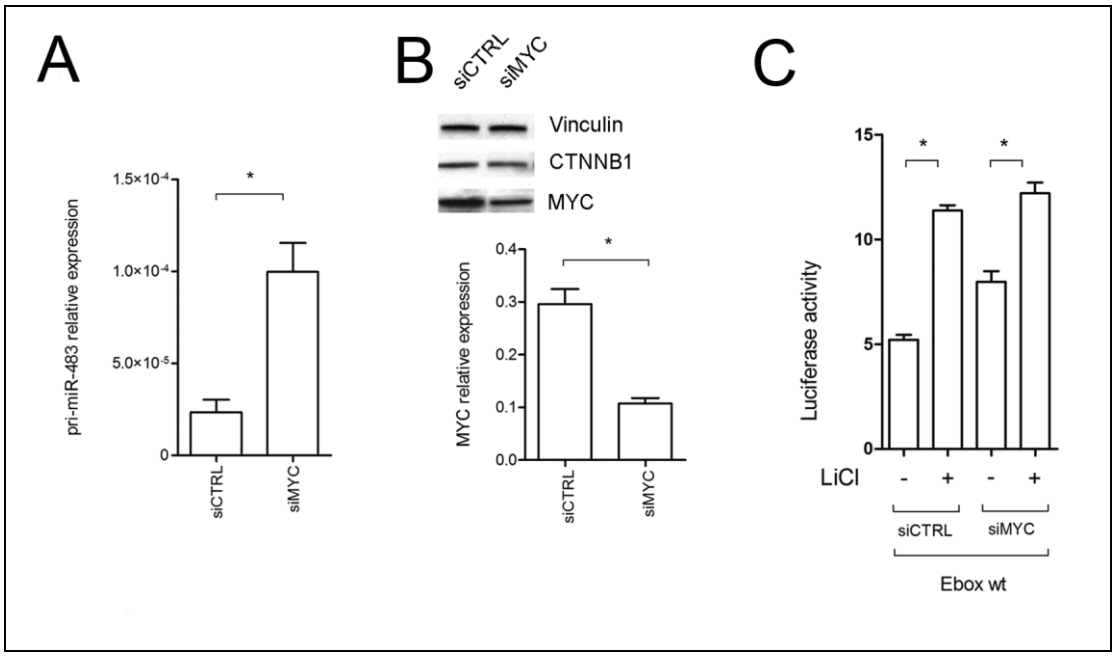


**Figure14.** MYC transcription factor repress miR-483 transcription. (**A**) PrimiR-483 expression in HEK293 cells transfected with siRNA control (siCTRL) and specific a siRNA for MYC (siMYC), (**B**) on the same samples the MYC and CTNNB1 protein were assessed by western blot to ensure the MYC silencing and that CTNNB1 was not involved in this experiment (upper panel). The lower panel shows the MYC mRNA expression by qRT-PCR. (**C**) Luciferase activity of the pGL4E_Ebox wild type (wt) with and without treatment with LiCl in HEK293 cells transiently knocked down for MYC by siRNA (siMYC). Firefly luciferase activity was normalized on Renilla luciferase activity of the cotransfected pGL4R vector. Single asterisk indicates a p value<0.02, double asterisk indicates a p value >0.02.

Then I determined whether MYC is the β-catenin mediator for *miR-483* transcriptional activation. Since MYC is well expressed in HEK293 cells I knocked-down its expression using a specific siRNA and measured the relative expression of the precursor of miR-483 (pri-miR-483). Unexpectedly, this resulted in an increase in the expression of pri-miR-483 (**Figs 14A-B**). Similar results were obtained by a luciferase assay using the pGL4E-Ebox

reporter vector in cells cotransfected with siRNA for MYC. These data indicate that MYC is not the responsible for the activation of the miR-483 locus after β-catenin activation because of its suggested repressive role on miR-483 transcription.

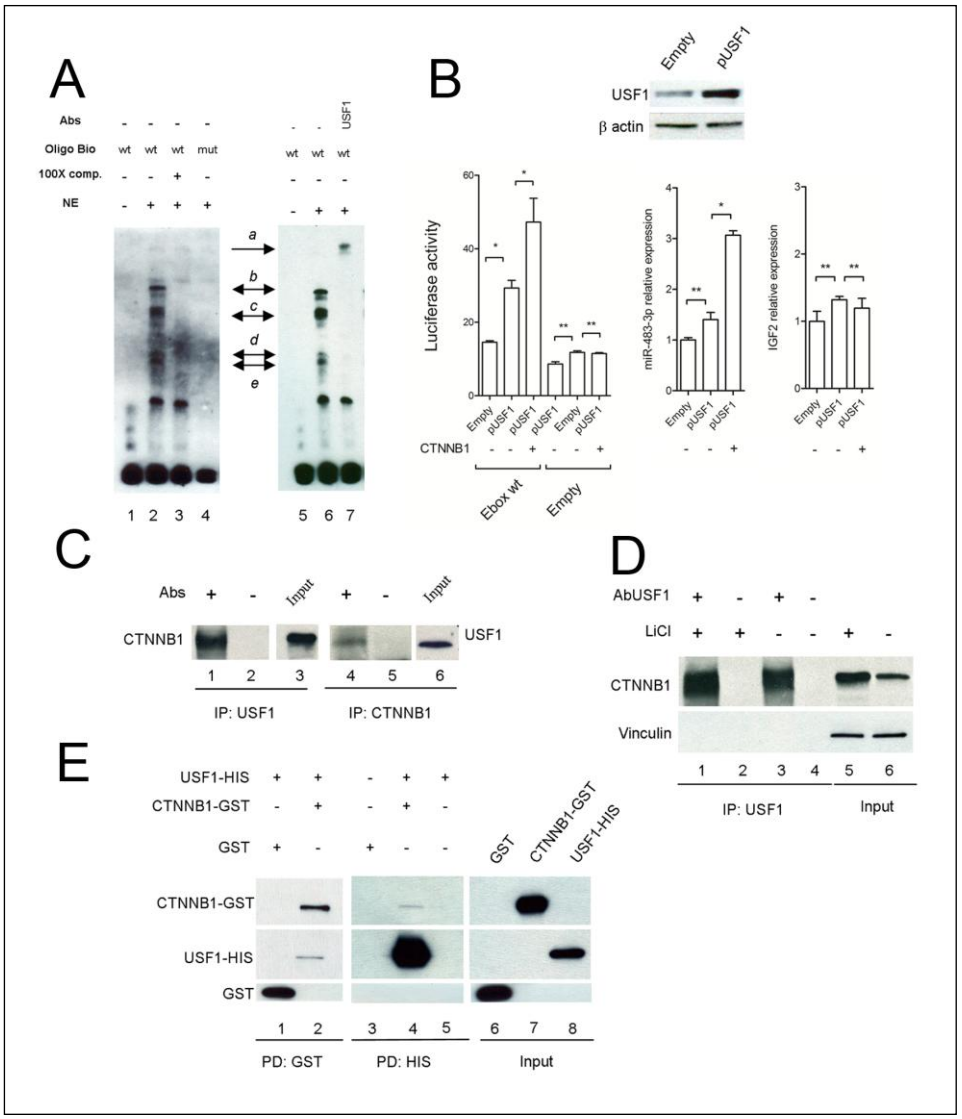


**Figure 15. USF1 serves a mediator between β-catenin and the miR-483 locus.** (**A)** EMSA of nuclear extract from HEK293 cells using the miR-483 Ebox probe. (lane 1-3, 5-7) or the mutant form (lane 4). The specific complexes are indicated by black arrows (*b,c,d* and *e*). Lane 7 shows the supershift generated by USF1 antibody (complex *a*). (**B**) Luciferase assay of pGL4E_Ebox wild type after enforced expression of USF1 and CTNNB1 using the pGL4E empty vector as control (left panel). The middle and right panels show the expression of miR-483-3p and IGF2 gene, respectively, after enforced expression of USF1 and CTNNB1. The miR-483-3p and IGF2 expression value of the empty vector were the controls. The exogenous expression of USF1 was assessed by western blot (upper panel). (**C**) Nuclear extract from HEK293 were immunoprecipitated with either USF1 (lanes 1-3) and CTNNB1 antibodies (lanes 4-6). After being washed, samples were run on SDS-PAGE gel and transferred to nitrocellulose. The blots were probed with USF1 and CTNNB1 antibody. (**D**) Nuclear extract from HEK293 with (lanes 1, 2) and without (lanes 3, 4) treatment with LiCl (20 mM for 24h) were imunoprecipitated with USF1 antibody and the blot probed for CTNNB1 protein. The Input shows an incremented quantity of CTNNB1 after LiCl treatment (lanes 5, 6). Vinculin protein expression was used as loading protein control. (**E**) GST-CTNNB1 and HIS-USF1 fusion proteins were subjected to GST (lanes 1,2) and HIS (lanes 3-5) pull-down analysis. Binding reaction products were washed, and proteins were separated by SDS-PAGE. The membrane was probed with both anti-CTNNB1, anti-USF1 and and GST antibodies. Single asterisk indicates a p value<0.02, double asterisk indicates a p value >0.02.

Since the Ebox element can also bind to the Upstream Stimulating Transcription Factor 1 (USF1) I tested this interaction by Electrophoretic Mobility Shift (EMSA) and Super Shift assays, although no previous connection between USF1 and β-catenin has been shown. USF1 is an evolutionary well conserved and ubiquitously expressed transcription factor involved in a wide number of cellular activities such as immune response, cell cycle and proliferation, and lipid and glucose metabolism [60]. As shown in **Figure 15A** the EMSA assay generates a specific band shift pattern (complex *b* to *e*, lane 2, **Fig 15A**) that disappears in the mutant form of the Ebox element oligonucleotide (lane 4, **Fig 15A**). Moreover, by using the anti-USF1 antibody, a super-shift complex was generated (complex *a*, lane 7, **Fig 15A**) suggesting that USF1 recognizes the Ebox element upstream of the *miR-483* locus.

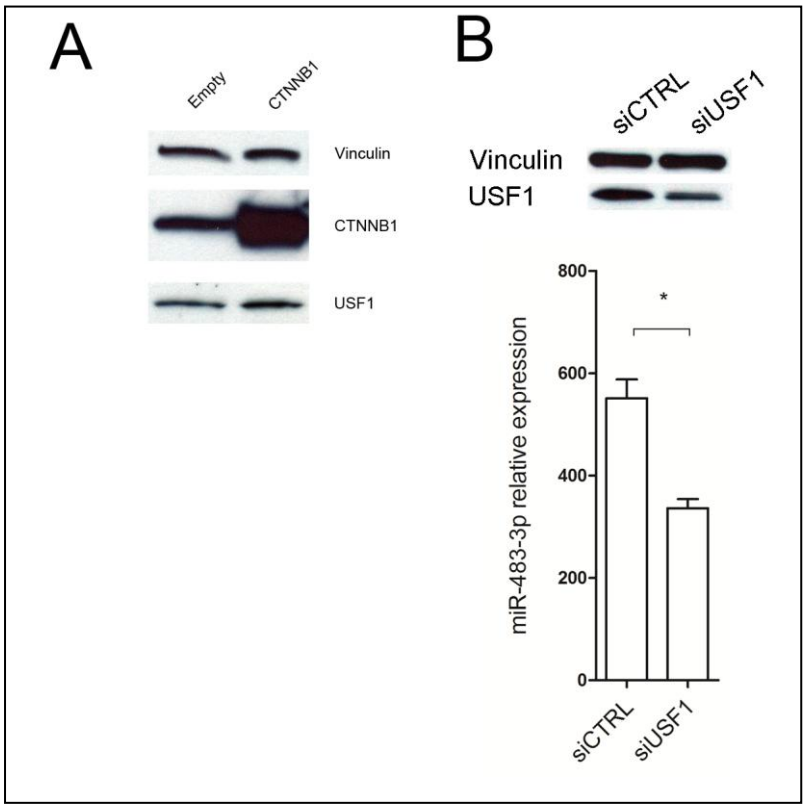


**Figure 16. (A)** Western blot analysis of β–catenin and USF1 in HEK293 cells transfected with the β–catenin expression vector. Vinculin was used as protein load control **.(B)** Western blot analysis of USF1 protein in HepG2 cells transfected with USF1 siRNA at 72 hours from transfection (upper panel) and the corresponding *miR-483-3p* relative expression (lower panel). Single asterisk indicates a p value<0.02, double asterisk indicates a p value >0.02.

To confirm this result I cloned the coding sequence of the USF1 gene into pCMV-Tag vector and co-transfected it into HEK293 cells along with pIRES-Neo β-catenin and the reporter vector pGL4E-6841-6910 with a wild type or mutant E-box (**Fig 15B** left panel). USF1 over expression was able to induce luciferase activity (2 fold) that was further increased in the presence of exogenous β-catenin (about 3 fold) compared to the control. Similar results obtained by RT-qPCR for *miR-483-3p* showed that *miR-483-3p* was weakly induced by exogenous USF1 (p=0.05) but increased about 3 times with co-expression of USF1 and

CTNNB1 ($p<0.02$) (**Fig 15B** middle panel). Note that IGF2 expression was unchanged (**Fig 15B** right panel). To exclude a transcriptional regulation of USF1 by β-catenin, Ialso tested that the USF1 protein level after β-catenin enforced expression was not changed (**Fig.16A**).

These data suggest USF1 is an important mediator of the regulation of *miR-483* locus driven by the β-catenin. To further confirm these results, Itransiently knocked-down USF1 by siRNA in HepG2 cells that show a very high β-catenin activity and miR-483-3p expression. qRT-PCR verified a significant reduction of *miR-483-3p* expression, compared to the control, after 72 hours from siRNA transfection (**Fig.16B**). These data suggest USF1 is an important mediator of the regulation of *miR-483* locus driven by the β-catenin.

**β-catenin and USF1 directly interact.** To understand the interplay between β-catenin and USF1 I tested the possibility of interaction between these two proteins. I co-immunoprecipitated from HEK293 nuclear extract lysate with either an anti-USF1 antibody or an anti-β-catenin antibody then immunoblotted with either anti-β-catenin or anti-USF1, respectively and found the two proteins co-immunoprecipitated (**Fig 15C**). Since LiCl treatment is able to induce miR-483 locus expression I tested the ability of β-catenin to co-immunoprecipitate with USF1 with and without LiCl treatment. Western blot analysis revealed an increased quantity of β-catenin immunoprecipitated with anti-USF1 (22%) compared to the non-treated control (**Fig 15D**) where the induction of β-catenin protein level after LiCl treatment was increased about 60%.

Then I tested whether these two proteins have the ability to directly interact by using the purified proteins CTNNB1-GST and USF1-HIS in pull-down assays. Both the pull-down assays revealed direct interaction between the two proteins (**Fig 15E**).

**miR-483-3p reveals a negative regulative loop by targeting β-catenin.** Since regulative feed-back loops between microRNAs and their targets have been shown in numerous cases [61] [62] [63] I investigated the possibility that β-catenin and/or USF1 are targets of *miR-483-3p* or *5p*. By *in-silico* analysis (http://targetscan.org/) I found that CTNNB1 is a predicted target of the *miR-483-3p* (**Fig 17A**).

To test the direct interaction of *miR-483-3p* with the CTNNB1 3'UTR, either the predicted *miR-483-3p* target site of the CTNNB1 mRNA, or a mutated target site used as a negative control was cloned downstream of the luciferase reporter gene in the pGL3-Control vector. These *miR-483-3p* responsive vectors were co-transfected into HEK293 and HCT116 cells

with either an RNA oligonucleotide *miR-483-3p* mimic or a scrambled sequence. A renilla luciferase vector (pGL4R) was used as a reference normalization control. In comparison with the control vector, the *miR-483-3p* caused a decrease in luciferase activity of about 30% and 50% in HEK293 and HCT116 respectively, whereas in the mutated 3'UTR clones luciferase activities were not perturbed by *miR-483-3p* (**Fig 17B**).

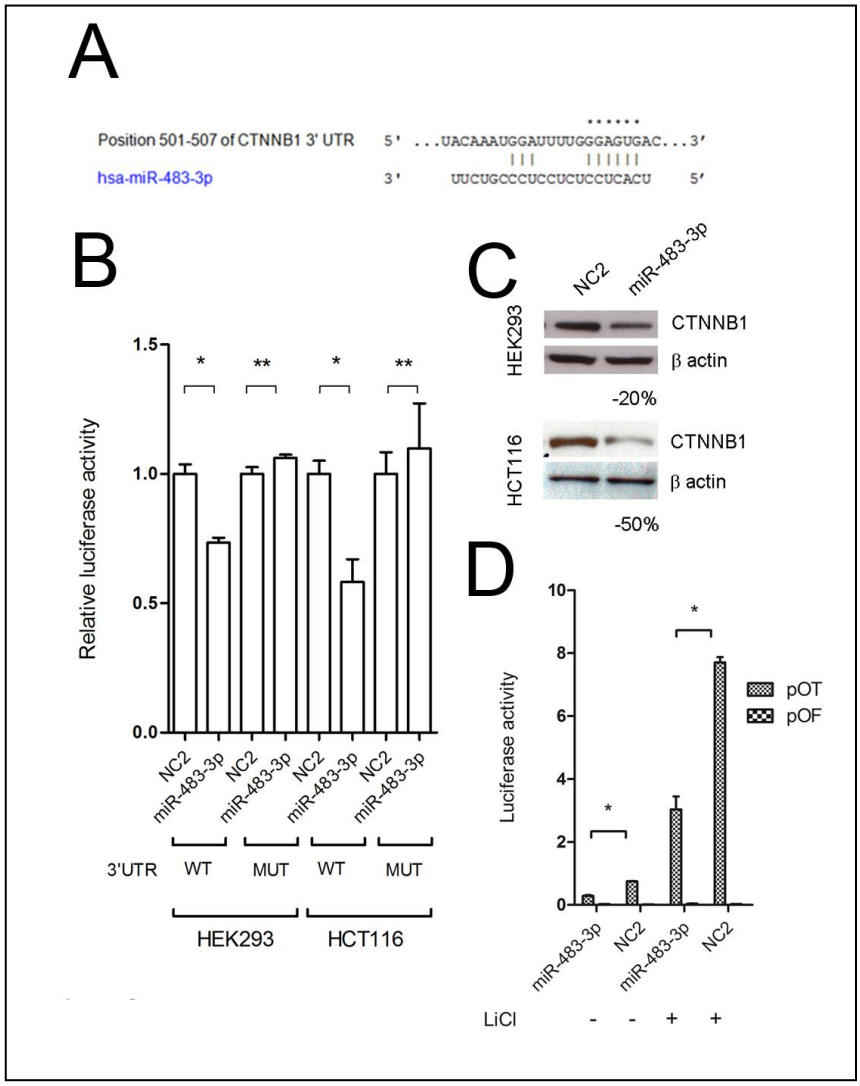


**Figure 17. β-catenin is a target of miR-483-3p.** (**A**) Putative binding site of *miR-483-3p* in CTNNB1 3'UTRs (TargetScan Database). Asterisks show nucleotides substituted in 3'UTR miR-483-3p predicted target site to perform luciferase assay. (**B**) CTNNB1 3'UTRs regulates luciferase activity dependent on *miR-483-3p* in HEK293 and HCT116 cell lines (WT, wild type; MUT, mutant). (**C**) Western blot analysis of CTNNB1 after *miR-483-3p* transfection in HEK293 and HCT116 cell line. Cells were collected after 48 hours after miRNA transfection. (**D**) Luciferase activity of the reporter vectors pOT and pOF in HCT116 co-transfected with miR-483-3p and scramble oligo (NC2) with and without LiCl treatment. Single asterisk indicates a p value<0.02, double asterisk indicates a p value >0.02.

To further confirm β-catenin as target of *miR-483-3p*, the protein level was assessed by western blot of HEK293 and HCT116 cells transfected with *miR-483-3p*. Protein expression was reduced about 20% and 50% when compared to negative control (**Fig 17C**). Moreover, in HCT116 cells that harbour a mutated β-catenin, the co-transfection of *miR-483-3p* and the reporter vector pGL3-OT revealed a functional reduction of nuclear β-catenin of

approximately 60% compared to the controls, with or without LiCl (**Fig 17D**). These data prove that *miR-483-3p* can inhibit β-catenin transcriptional activity.

**The mutated form of β-catenin can evade the *miR-483-3p* regulative loop.** Our findings suggest a negative regulatory loop between *miR-483-3p* and β-catenin exists. However both genes are over-expressed or have higher activity in tumors, suggesting that β-catenin could escape miR-483-3p regulation. Since it has been described that a single nucleotide polymorphism (SNP) within the 3'UTR of the β-catenin mRNA target could affect the binding of the miRNA [64 65 66] I analyzed the mutational status of the β-catenin 3'UTR in 8 cell lines (RD, MCF7, RKO, SK-NEP1, G401, A204, U2OS, HEK293) and 30 Wilms' tumor samples. I found 2 SNPs, rs2953 and rs4135387 that I cloned into pGL3-control and tested for their susceptibility to *miR-483-3p* regulation by a luciferase assay. No significant differences were found (**Fig.18**).I also determined that *miR-483-3p* was not mutated in these samples. This result led us to speculate that mutations in the coding sequence of β-catenin may be affecting this process.

**Figure 18.** CTNNB1 3'UTRs regulates luciferase activity dependent on *miR-483-3p* in HEK293 independently of the SNPs rs2953 and rs 4135387 when compare to the reference sequence wild type. Firefly luciferase activity was normalized on Renilla luciferase activity of the cotransfected pRL-TK vector. Single asterisk indicates a p value<0.02, double asterisk indicates a p value >0.02.

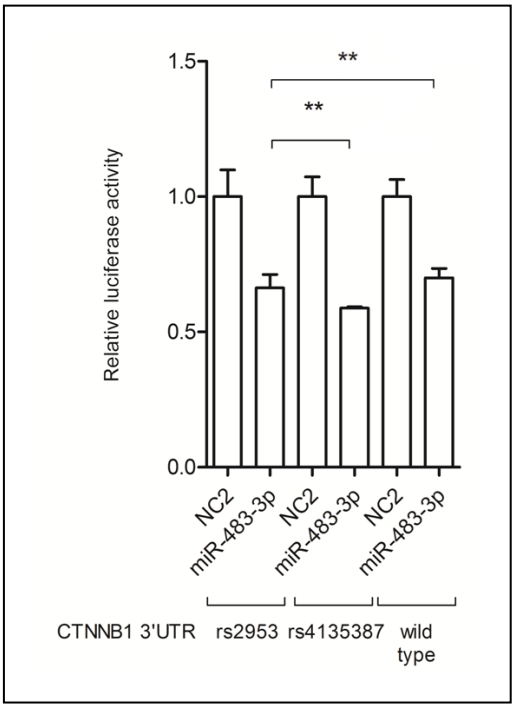

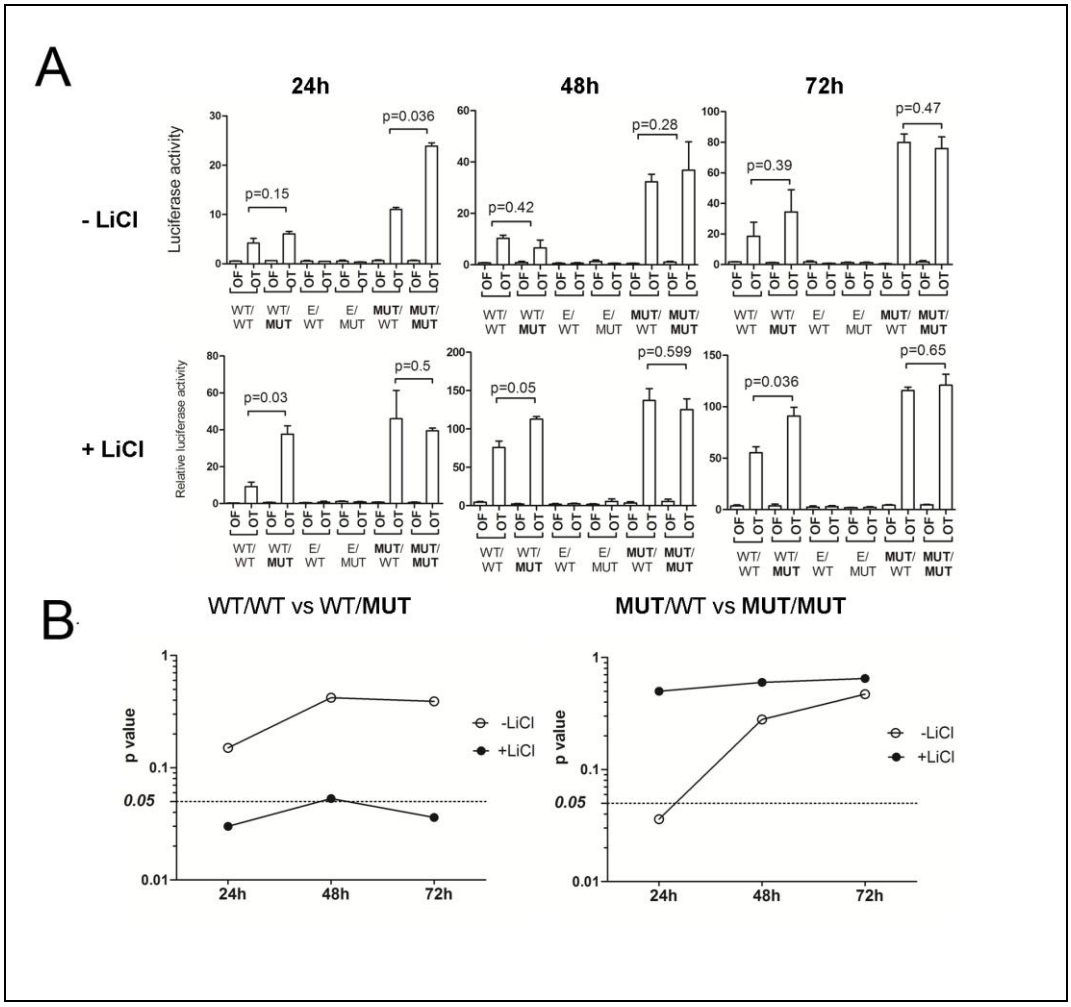


**Figure 19 The mutated form of β-catenin evades the *miR-483-3p* regulative loop.** (**A**) Luciferase activity during the time (24, 48, 72 hours) of the reporter vectors pOT and pOF in HEK293 co-transfected with the 4 different CTNNB1 expression vectors (mutational status of the CDS and 3'UTR miR-483-3p target site of CTNNB1: CDS/3'UTR) with (lower panel) and without LiCl treatment (upper panel). As experiment controls the CTNNB1 3'UTR wild type and mir-483-3p target mutated were cloned in the expression vector pIRESNeo2: Empty/WT (E/WT) and Empty/MUT (E/MUT). The p-values are indicated and graphically represented in ***B***.

I cloned either the wt β-catenin 3'UTR or the 3' UTR with a mutated *miR-483-3p* target site into two different pIRES-Neo2 β-catenin expression vectors, one with wt β-catenin and the other with a Ser45 deletion. As a control vector with only the 3'UTR and no coding sequence was used. The 6 combinations of vectors were transfected into HEK293 cells and β-catenin nuclear activity was measured by the pGL3-OT (list the pGL3-OF in figure legend) luciferase reporter vector after 24, 48 and 72 hours. This allowed evaluation of the 2 different types of negative regulation of β-catenin (GSK3B mediated degradation and *miR-483-3p* mediated translational inhibition). After transfection in HEK293 cells all forms of β-catenin were able

to increase the luciferase activity of the pGL3-OT at 24, 48 and 72 hours compared to the controls (**Fig 19A**) however I did not seen any significant difference between the WT/WT and WT/MUT forms (CDS/3'UTR). This could be due to the high rate of GSK3B-mediated β-catenin degradation which is strong in HEK293 cells and could hide the effect of *miR-483-3p*. To overcome this problem the experiment was conducted in the presence of LiCl which resulted in a significant increase of activity in the presence of the WT/MUT but not the WT/WT form suggesting that the wt 3' UTR is controlled by *miR-483-3p*, but the mutant form is not (**Fig 19A** and **Fig 19B**, left panel). On the other hand the Ser45 mutant form of β-catenin showed a significant difference in regulation by *miR-483-3p* at the 3'UTR (MUT/WT vs MUT/MUT) only at 24 hours without LiCl ($p=0.036$). Since the mutant form is not degraded and thus accumulates in the cells, it is reasonable that at an early time point β-catenin protein levels are still controlled by *miR-483-3p* but this regulation is lost over time (**Fig 19B**, right panel). Taken together these data support that the activating mutation of β-catenin results in loss of regulation by *miR-483-3p*.

## Discussion

I established a link between *miR-483-3p*, a miRNA located within the *IGF2* locus at chromosome 11p15.5, and human tumorigenesis. Various evidences support this conclusion. First, tumorigenicity of HepG2, a cell line that over-expresses *miR-483-3p*, is suppressed by AMO anti-miR-483-3p; second, the miRNA is up-regulated and over-expressed in Wilms' tumors, as well as in common human neoplasms; third, *miR-483-3p* supports cell survival by protecting cells from apoptosis; fourth, an important regulator of apoptosis, Puma, is inhibited by the expression of *miR-483-3p.*

To demonstrate the oncogenic properties of *miR-483-3p*, I proved that silencing of *miR-483-3p* by AMO could reduce tumorigenicity of HepG2 cells, a cell line that exhibits high expression of the *IGF2/miR-483* locus and functional activity of IGF2 ligand [67] [68]. Importantly, the reduction in tumor formation by the specific silencing of *miR-483-3p* was achieved without changing *IGF2* gene expression. Moreover, the silencing of the *IGF2* gene by siRNA technologies did not cause a significative changing in tumors formation by HepG2 cells. These results clearly indicate that a crucial oncogenic function associated with the *miR-483-3p* miRNA within the *IGF2* locus. This conclusion may explain why transgenic animal models for *Igf2* over-expression did not develop tumors [21]. In fact, these animal models were developed by using an *Igf2* cDNA, which lacked the *mir-483* locus. It could be speculated that, by protecting cells from apoptosis, *miR-483-3p* provides the additional element required for supporting malignant transformation promoted by the growth factor IGF2. Indeed, in Wilms' tumor, HCC and CRC studied the expression of the *IGF2/miR-483* locus is co-regulated in almost all the samples analyzed. Interestingly, some cases present a divergent expressions of *miR-483-3p* and *IGF2*, suggesting a possible *IGF2* independent mechanisms of *miR-483-3p* regulation.

By proving that ectopic expression of *miR-483-3p* can protect cells from apoptosis, while inhibition of endogenous *miR-483-3p* increases basal or induced apoptosis, I demonstrate that the up-regulation of *miR-483-3p* can protect cells from apoptosis. This is in line with the finding that *miR-483-3p* can target and repress the expression of the pro-apoptotic protein PUMA, a BH3-only protein, whose induction is mediated by p53 [46,69]. Like other BH3-only proteins, it promotes apoptosis by interacting and inhibiting the anti-apoptotic factors BCL2 and BCLXL [69-71]. Hence, an over-expressed *miR-483-3p* may favor cell survival by reducing the level of Puma after P53 activation during apoptosis stimuli, and therefore acting as an anti-apoptotic oncogene. These results support this conclusion.

The involvement of *miR-483-3p* in cancer is supported by the observation that is over-expressed in about 30% of common human cancers and in 100% of Wilms' tumors. In addition, Guled et al. reported the up-regulation of *miR-483-3p* in malignant mesothelioma [41]. In human cancers the over-expression of *miR-483-3p* could be linked to its co-regulation with *IGF2* expression. Interestingly, through this mechanism, both growth, IGF2, and survival stimuli, *miR-483-3p,* are simultaneously activated.

However some tumor samples displayed a divergent expression between *IGF2* and *miR-483-3p*, thus revealing the existence of mechanisms where *IGF2* and *hsa-mir-483* are not co-regulated. Therefore I investigated also this aspect of the research. I identified a new molecular mechanism of auto-regulation of β-catenin activity through *miR-483-3p,* and a novel interaction between the transcription factors USF1 and β-catenin. After genetic analysis of HCC samples, I identified an association between the activation of the β-catenin pathway and the over-expression of *miR-483-3p,* an association that was stronger in a subset of samples that exhibited a divergent expression between *IGF2* and *miR-483-3p*. This observation was supported by the finding that the *miR-483* locus could be up-regulated independently from its host gene *IGF2* by enforced over-expression of β-catenin.

These findings indicate the existence of at least two mechanisms responsible for the expression of *miR-483-3p*: co-regulation with *IGF2* and transcriptional induction by β-catenin. The first mechanism appears to be significantly represented in Wilms' tumors and possibly other pediatric tumors. In these tumors, the well-known over-expression and loss of imprinting of *IGF2* may be responsible for most of the *miR-483* up-regulation. Through this mechanism, both cell growth and survival can be simultaneously stimulated by *IGF2* and *miR-483-3p,* respectively. The second mechanism may explain the over-expression of *miR-483-3p* in adult human cancers, where its up-regulation may occur independently from *IGF2* expression.

The mediator of *miR-483* stimulation by β-catenin was identified as the basic Helix-Loop-Helix Upstream Stimulating factor USF1. Here, I prove that it can directly interact with β-catenin and recognize the E-box CACGTG element located 400 nucleotides upstream of the *miR-483* locus. The interaction between β-catenin and another bHLH protein, MyoD, was previously described [72], but this is the first demonstration of the direct interaction between β-catenin and USF1. USF1 is a widely expressed transcription factor that plays a crucial role in the regulation of cell cycle and proliferation [73,74] and gluco-lipidic metabolism. [75,76].

Moreover has been shown USF1 plays also an important role for the maintenance of a chromatin barrier at the insulator elements of the chicken β-globin gene [77].

The recent demonstration of the safe and effective use of anti-miRNAs in animal models, including African green monkeys, suggest the potential application of AMOs also in anti-cancer therapy [78,79]. Our findings indicate the *miR-483-3p* as a potential target for anti-neoplastic intervention in Wilms' and possibly many other tumors. Thus, these results not only improve our understanding on the molecular mechanisms involved in tumor development, but they also provide indication for a novel potential therapeutic target.

My discovery of a negative regulative loop between *miR-483-3p* and β-catenin generates an apparent paradox. To explain this discrepancy, I found that the mutated form of β-catenin is able to evade *miR-483-3p* regulation and the mutated protein can still accumulate in the cell.

In addition to the β-catenin-USF1 / *miR-483* mechanism, in this study I found that CTCF can also participate in the regulation of *miR-483* expression. Indeed, I confirmed data published by Du et al. [53], who found that the region immediately upstream of the *miR-483* locus binds the multifunctional protein CTCF. I found evidence that CTCF could play an important role in the regulation of *miR-483* locus as a transcriptional repressor and that repression is indirectly correlated to the methylation status of a CpG dinucletide in the CTCF binding site. CTCF is a well known regulator of imprinted regions of the genome such as the *IGF2/H19* locus where it permits the monoallelic expression of these two genes [80,81] by modulating the conformation of this region, which [82] affects transcriptional activity. It is also important to note that the chromosomal region where CTCF is located (16q21) is often deleted in Wilms' tumor [83,84]. Our finding highlights the role of the miR-483 locus as point of junction among the most important players in Wilms' tumor (*IGF2* locus, Wnt/β-catenin pathway and *CTCF*).

By unraveling the complex regulation of the *miR-483* locus, the present study provides new insight into the Wnt/β-catenin pathway and indicates new targets for anticancer therapy.

## Conclusion and future perspectives

Hsa-miR-483 is located within intron 2 of the IGF2 locus. IGF2 is a fetal growth factor whose abnormally high expression has been associated with the development of nephroblastoma, hepatoblastoma and rhabdomyosarcoma. I found that *miR-483-3p* is overexpressed in all the Wilms' tumors I studied. In addition, colon, breast, and liver cancers exhibit high or even extremely levels of miR-483-3p in ~30% of the cases. Functionally I found that the miR-483-3p acts as an oncomiR by targeting the pro-apoptotic gene p53 up-regulated modulator of apoptosis (BBC3/PUMA) [40,85].

The significance of these finding is related to the genomic position of this miRNA that maps at the second intron of *IGF2* gene on the 11p15.5 chromosomal region called *WT2* region (Wilms' tumor region 2) and/or *MTACR1* (Multiple Tumor-Associated Chromosomes Region1) because of its involvement in several tumors. IGF2 gene has been studied for many years in connection to Wilms' tumor [86] and Beckwith-Wiedemann syndrome (BWS) and it was found upregulated. Nevertheless IGF2 murine transgenic models have highlighted features close to the Beckwith-Wiedemann syndrome [21] without tumor predisposition. Recently Hu et al. published a Wilms' tumor mouse model caused by somatic ablation of Wt1 and constitutional up-regulation of Igf2 locus [87]. Taken together these results suggest an important cooperation between IGF2 and miR-483, their co-presence stimulate both cell growth and survival in cancer cells.

Generally a co-regulation of IGF2 and miR-483 was registered even though I identified a second regulatory mechanism of miR-483 independently of IGF2 expression. MiR-483 locus could be regulated by a novel transcription complex that involves the onco-protein β-catenin and the upstream transcription factor 1 (USF1). The β-catenin\Wnt pathway is one of the most important pathway dysregulated in cancer and USF1 is an evolutionary well conserved and ubiquitous transcription factor (TF) involved in a wide number of cellular activities such as cell cycle and proliferation, and lipid and glucose metabolism [60].

I identify the TF CMYC as repressor of the miR-483 locus. This finding could explain the pro-apoptotic character of this oncogene [88,89]and the interesting result obtained by Okuyama et al. They show that c-MYC protein levels cancer cells in vivo are strikingly reduced in the area distant from the blood vessels enhancing cell survival [90].

### Description of preliminary data

1. **MYC transcription factor represses miR-483 expression**. I recently published an auto-regulative loop between miR-483 and β-catenin transcription factor by the novel interaction β-catenin/USF1. During this study I found that CMYC repress the transcription of miR-483.

HEK293 cells knocked down for CMYC by short interfering RNA show an incremented expression of the pri-miR-483 (**Fig.14A-B**). These data suggest that CMYC is involved at the transcription step of the locus and not during the maturation of the miRs considered. Luciferase assay to evaluate the promoter region of the miR-483 locus highlight that the CMYC repression is independent from the USF1 binding site (same recognition sequence of CMYC) (**Fig.14C).**

By Chromatin immunoprecipitation analysis I found that CMYC bounds the miR-483 promoter (**Fig.20B).** Has been published that the CMYC repressive function is exerted by the mediator myc-interacting zinc finger protein 1 (MIZ-1) [91], since I found 4 MIZ-1's predicted binding in the 500 bp up-stream the miR-483 locus (**Fig.20A)** I suppose an involvement of this protein in the regulation of miR-483.

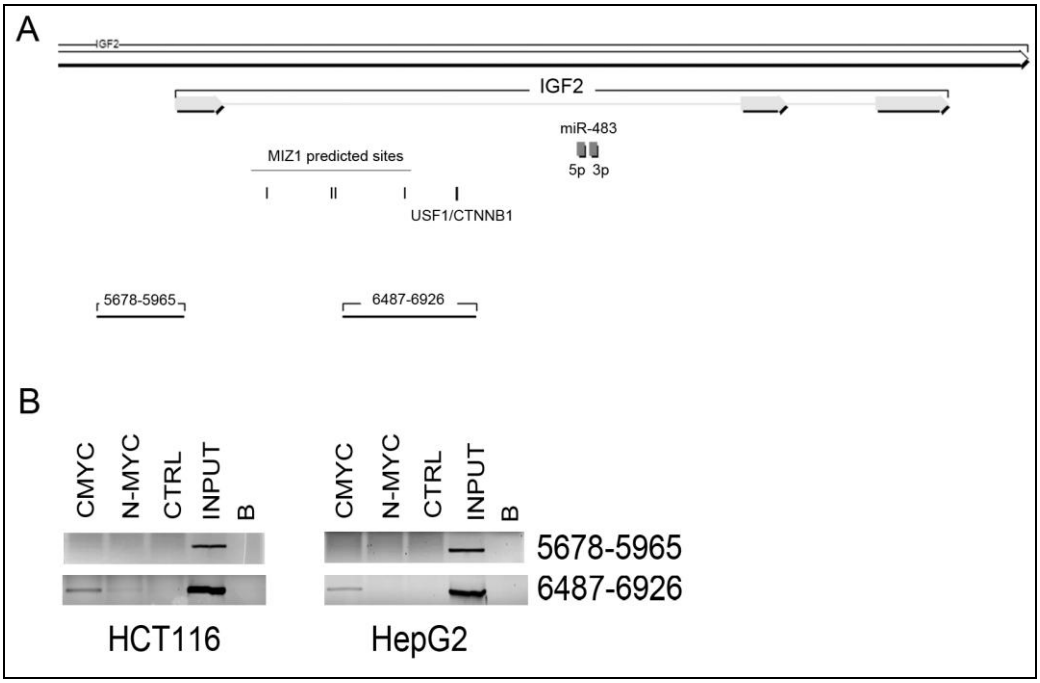


**Fig.20** **(A**) Genomic structure of IGF2/483 locus from the reference AF517226 genomic sequence. IGF2's Exons (gray bars), the four predicted MIZ1 binding sites (black bars), miR-483-3p and miR-483-5p (dark gray boxes) are shown. Are indicated the 2 genomic fragments amplified for the ChIP analysis. (**B**) ChIP analysis using CMYC and NMYC antibibodies in HepG2 and HCT116 cell lines (B indicates the blank of the PCR).

2. **Glucose influences miR-483-3p expression.** Since I found USF1 regulates miR-483 expression [85] and that USF1 is regulated by glucose [92,93] I evaluated miR-483-3p expression in HepG2 cells deprived of glucose. As shown in figure 21 the expression of miR-483-3p is gradually down-regulated during the time in cells deprived of glucose. On the other hand in presence of glucose the expression of miR-483-3p seems increased over time. The down-

regulation of miR-483-3p coincides with a down-regulation in the protein level of β-catenin but USF1 seems not influenced (data not shown).

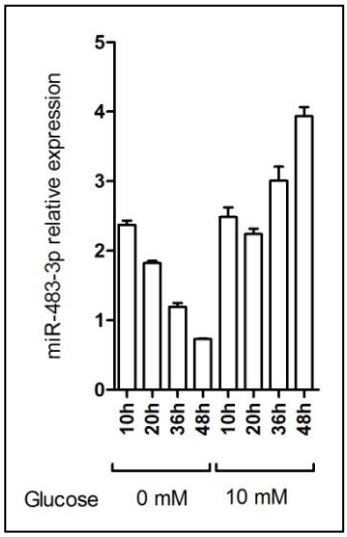


**Fig. 21** Time course of miR-483-3p relative expression on HepG2cells cultured with and without glucose (0mM and 10mM). The miR-483-3p expression was normalized to the endogenous reference RNU6B

I support the hypothesis that the glucose metabolism could be an important factor in the regulation of the anti-apoptotic miR-483-3p, given the 1) location of miR-483 in the INS-IGF2 gene in the 11p15.5 chromosome region, 2) the involvement of USF1 that seems to be necessary to the glucose response [92], 3) the β-catenin/Wnt pathway that is regulated by the glycogen synthase kinase 3 beta (GSK3B), 4) the inhibition of glucose metabolism is described to be an apoptotic stimulus [94,95] and 4) our preliminary data that show a down-regulation of miR-483 in HepG2 cells cultured in absence of glucose.

My future aim is to draw the complex scenario of the regulation of miR-483 locus to identify new possible approaches in the treatment of cancers that exhibit miR-483 up-regulation. Our preliminary data suggest the involvement of glucose metabolism in the miR-483 regulation, moreover I published the involvement of the transcriptional factors USF1 and CMYC in the miR-483 regulation that are described implicated in glucose metabolism [96 97]. Since the anti-apoptotic role of miR-483-3p I suppose that inhibiting the pathway glucose metabolism I could improve the drug susceptibility of tumorigenic cells with elevated miR-483 expression.

## References


1 Fearon, E. R., Vogelstein, B. & Feinberg, A. P. Somatic deletion and duplication of genes on chromosome 11 in Wilms' tumours. *Nature* **309**, 176-178 (1984).

2 Koufos, A. *et al.* Loss of alleles at loci on human chromosome 11 during genesis of Wilms' tumour. *Nature* **309**, 170-172 (1984).

3 Orkin, S. H., Goldman, D. S. & Sallan, S. E. Development of homozygosity for chromosome 11p markers in Wilms' tumour. *Nature* **309**, 172-174 (1984).

4 Reeve, A. E. *et al.* Loss of a Harvey ras allele in sporadic Wilms' tumour. *Nature* **309**, 174-176 (1984).

5 Satoh, Y. *et al.* Genetic and epigenetic alterations on the short arm of chromosome 11 are involved in a majority of sporadic Wilms' tumours. *Br J Cancer* **95**, 541-547 (2006).

6 Ali, I. U., Lidereau, R., Theillet, C. & Callahan, R. Reduction to homozygosity of genes on chromosome 11 in human breast neoplasia. *Science* **238**, 185-188 (1987).

7 Fearon, E. R., Feinberg, A. P., Hamilton, S. H. & Vogelstein, B. Loss of genes on the short arm of chromosome 11 in bladder cancer. *Nature* **318**, 377-380 (1985).

8 Weston, A. *et al.* Differential DNA sequence deletions from chromosomes 3, 11, 13, and 17 in squamous-cell carcinoma, large-cell carcinoma, and adenocarcinoma of the human lung. *Proc Natl Acad Sci U S A* **86**, 5099-5103 (1989).

9 Lee, J. H., Kavanagh, J. J., Wharton, J. T., Wildrick, D. M. & Blick, M. Allele loss at the c-Ha-ras1 locus in human ovarian cancer. *Cancer Res* **49**, 1220-1222 (1989).

10 Rainier, S. *et al.* Relaxation of imprinted genes in human cancer. *Nature* **362**, 747-749 (1993).

11 Schwienbacher, C. *et al.* Abnormal RNA expression of 11p15 imprinted genes and kidney developmental genes in Wilms' tumor. *Cancer Res* **60**, 1521-1525 (2000).

12 Scelfo, R. A. *et al.* Loss of methylation at chromosome 11p15.5 is common in human adult tumors. *Oncogene* **21**, 2564-2572 (2002).

13 Poirier, K. *et al.* Loss of parental-specific methylation at the IGF2 locus in human hepatocellular carcinoma. *J Pathol* **201**, 473-479 (2003).

14 Haruta, M. *et al.* Duplication of paternal IGF2 or loss of maternal IGF2 imprinting occurs in half of Wilms tumors with various structural WT1 abnormalities. *Genes Chromosomes Cancer* **47**, 712-727 (2008).

15 Vu, T. H., Chuyen, N. V., Li, T. & Hoffman, A. R. Loss of imprinting of IGF2 sense and antisense transcripts in Wilms' tumor. *Cancer Res* **63**, 1900-1905 (2003).

16 Sparago, A. *et al.* Mechanisms causing imprinting defects in familial Beckwith-Wiedemann syndrome with Wilms' tumour. *Hum Mol Genet* **16**, 254-264 (2007).

17 Diaz-Meyer, N. *et al.* Silencing of CDKN1C (p57KIP2) is associated with hypomethylation at KvDMR1 in Beckwith-Wiedemann syndrome. *J Med Genet* **40**, 797-801 (2003).

18 Satoh, A. *et al.* Epigenetic inactivation of class II transactivator (CIITA) is associated with the absence of interferon-gamma-induced HLA-DR expression in colorectal and gastric cancer cells. *Oncogene* **23**, 8876-8886 (2004).

19 Gallagher, E. *et al.* Gain of imprinting of SLC22A18 sense and antisense transcripts in human breast cancer. *Genomics* **88**, 12-17 (2006).

20 Bjornsson, H. T. *et al.* Epigenetic specificity of loss of imprinting of the IGF2 gene in Wilms tumors. *J Natl Cancer Inst* **99**, 1270-1273 (2007).
21 Sun, F. L., Dean, W. L., Kelsey, G., Allen, N. D. & Reik, W. Transactivation of Igf2 in a mouse model of Beckwith-Wiedemann syndrome. *Nature* **389**, 809-815 (1997).
22 Fu, H. *et al.* Identification of human fetal liver miRNAs by a novel method. *FEBS Lett* **579**, 3849-3854 (2005).
23 Perez-Moreno, M., Jamora, C. & Fuchs, E. Sticky business: orchestrating cellular signals at adherens junctions. *Cell* **112**, 535-548, doi:S0092867403001089 [pii] (2003).
24 Clevers, H. Wnt/beta-catenin signaling in development and disease. *Cell* **127**, 469-480, doi:S0092-8674(06)01344-4 [pii]
10.1016/j.cell.2006.10.018 (2006).
25 Wang, S. S. *et al.* Alterations of the PPP2R1B gene in human lung and colon cancer. *Science* **282**, 284-287 (1998).
26 Satoh, S. *et al.* AXIN1 mutations in hepatocellular carcinomas, and growth suppression in cancer cells by virus-mediated transfer of AXIN1. *Nat Genet* **24**, 245-250 (2000).
27 Major, M. B. *et al.* Wilms tumor suppressor WTX negatively regulates WNT/beta-catenin signaling. *Science* **316**, 1043-1046 (2007).
28 Morin, P. J. *et al.* Activation of beta-catenin-Tcf signaling in colon cancer by mutations in beta-catenin or APC. *Science* **275**, 1787-1790 (1997).
29 Devereux, T. R. *et al.* CTNNB1 mutations and beta-catenin protein accumulation in human hepatocellular carcinomas associated with high exposure to aflatoxin B1. *Mol Carcinog* **31**, 68-73 (2001).
30 Kusafuka, T., Miao, J., Kuroda, S., Udatsu, Y. & Yoneda, A. Codon 45 of the beta-catenin gene, a specific mutational target site of Wilms' tumor. *Int J Mol Med* **10**, 395-399 (2002).
31 Rubinfeld, B. *et al.* Binding of GSK3beta to the APC-beta-catenin complex and regulation of complex assembly. *Science* **272**, 1023-1026 (1996).
32 Mann, B. *et al.* Target genes of beta-catenin-T cell-factor/lymphoid-enhancer-factor signaling in human colorectal carcinomas. *Proc Natl Acad Sci U S A* **96**, 1603-1608 (1999).
33 Tetsu, O. & McCormick, F. Beta-catenin regulates expression of cyclin D1 in colon carcinoma cells. *Nature* **398**, 422-426, doi:10.1038/18884 (1999).
34 Eulalio, A., Huntzinger, E. & Izaurralde, E. Getting to the root of miRNA-mediated gene silencing. *Cell* **132**, 9-14 (2008).
35 Ambros, V. The functions of animal microRNAs. *Nature* **431**, 350-355, doi:10.1038/nature02871
nature02871 [pii] (2004).
36 Calin, G. A. & Croce, C. M. MicroRNA signatures in human cancers. *Nat Rev Cancer* **6**, 857-866 (2006).
37 Iorio, M. V. & Croce, C. M. MicroRNAs in cancer: small molecules with a huge impact. *J Clin Oncol* **27**, 5848-5856, doi:JCO.2009.24.0317 [pii]
10.1200/JCO.2009.24.0317 (2009).
38 Negrini, M., Ferracin, M., Sabbioni, S. & Croce, C. M. MicroRNAs in human cancer: from research to therapy. *J Cell Sci* **120**, 1833-1840 (2007).

39 Esquela-Kerscher, A. & Slack, F. J. Oncomirs - microRNAs with a role in cancer. *Nat Rev Cancer* **6**, 259-269 (2006).

40 Veronese, A. *et al.* Oncogenic role of miR-483-3p at the IGF2/483 locus. *Cancer Res* **70**, 3140-3149, doi:0008-5472.CAN-09-4456 [pii] 10.1158/0008-5472.CAN-09-4456 (2010).

41 Guled, M. *et al.* CDKN2A, NF2, and JUN are dysregulated among other genes by miRNAs in malignant mesothelioma -A miRNA microarray analysis. *Genes Chromosomes Cancer* **48**, 615-623 (2009).

42 Soon, P. S. *et al.* miR-195 and miR-483-5p Identified as Predictors of Poor Prognosis in Adrenocortical Cancer. *Clin Cancer Res* **15**, 7684-7692, doi:1078-0432.CCR-09-1587 [pii] 10.1158/1078-0432.CCR-09-1587 (2009).

43 Suzuki, H. *et al.* Epigenetic inactivation of SFRP genes allows constitutive WNT signaling in colorectal cancer. *Nat Genet* **36**, 417-422 (2004).

44 Fornari, F. *et al.* MiR-221 controls CDKN1C/p57 and CDKN1B/p27 expression in human hepatocellular carcinoma. *Oncogene* (2008).

45 Olek, A., Oswald, J. & Walter, J. A modified and improved method for bisulphite based cytosine methylation analysis. *Nucleic Acids Res* **24**, 5064-5066, doi:l60209 [pii] (1996).

46 Jeffers, J. R. *et al.* Puma is an essential mediator of p53-dependent and -independent apoptotic pathways. *Cancer Cell* **4**, 321-328 (2003).

47 Nusse, R. Cancer. Converging on beta-catenin in Wilms tumor. *Science* **316**, 988-989 (2007).

48 Reya, T. & Clevers, H. Wnt signalling in stem cells and cancer. *Nature* **434**, 843-850 (2005).

49 de La Coste, A. *et al.* Somatic mutations of the beta-catenin gene are frequent in mouse and human hepatocellular carcinomas. *Proc Natl Acad Sci U S A* **95**, 8847-8851 (1998).

50 Taniguchi, K. *et al.* Mutational spectrum of beta-catenin, AXIN1, and AXIN2 in hepatocellular carcinomas and hepatoblastomas. *Oncogene* **21**, 4863-4871 (2002).

51 Katoh, H. *et al.* Genetic inactivation of the APC gene contributes to the malignant progression of sporadic hepatocellular carcinoma: a case report. *Genes Chromosomes Cancer* **45**, 1050-1057 (2006).

52 Korinek, V. *et al.* Constitutive transcriptional activation by a beta-catenin-Tcf complex in APC-/- colon carcinoma. *Science* **275**, 1784-1787 (1997).

53 Du, M. *et al.* Insulator and silencer sequences in the imprinted region of human chromosome 11p15.5. *Hum Mol Genet* **12**, 1927-1939 (2003).

54 Kuhn, E. J. & Geyer, P. K. Genomic insulators: connecting properties to mechanism. *Curr Opin Cell Biol* **15**, 259-265, doi:S0955067403000395 [pii] (2003).

55 Jelinic, P. & Shaw, P. Loss of imprinting and cancer. *J Pathol* **211**, 261-268, doi:10.1002/path.2116 (2007).

56 Prawitt, D. *et al.* Microdeletion of target sites for insulator protein CTCF in a chromosome 11p15 imprinting center in Beckwith-Wiedemann syndrome and Wilms' tumor. *Proc Natl Acad Sci U S A* **102**, 4085-4090, doi:0500037102 [pii] 10.1073/pnas.0500037102 (2005).

57 Chan, C. S. & Song, J. S. CCCTC-binding factor confines the distal action of estrogen receptor. *Cancer Res* **68**, 9041-9049, doi:68/21/9041 [pii]

10.1158/0008-5472.CAN-08-2632 (2008).
58 Butcher, D. T. & Rodenhiser, D. I. Epigenetic inactivation of BRCA1 is associated with aberrant expression of CTCF and DNA methyltransferase (DNMT3B) in some sporadic breast tumours. *Eur J Cancer* **43**, 210-219, doi:S0959-8049(06)00800-8 [pii] 10.1016/j.ejca.2006.09.002 (2007).
59 Paradowska, A. *et al.* Aberrant epigenetic modifications in the CTCF binding domain of the IGF2/H19 gene in prostate cancer compared with benign prostate hyperplasia. *Int J Oncol* **35**, 87-96 (2009).
60 Corre, S. & Galibert, M. D. Upstream stimulating factors: highly versatile stress-responsive transcription factors. *Pigment Cell Res* **18**, 337-348, doi:PCR262 [pii] 10.1111/j.1600-0749.2005.00262.x (2005).
61 Petrocca, F. *et al.* E2F1-regulated microRNAs impair TGFbeta-dependent cell-cycle arrest and apoptosis in gastric cancer. *Cancer Cell* **13**, 272-286, doi:S1535-6108(08)00049-4 [pii] 10.1016/j.ccr.2008.02.013 (2008).
62 Yang, X. *et al.* miR-449a and miR-449b are direct transcriptional targets of E2F1 and negatively regulate pRb-E2F1 activity through a feedback loop by targeting CDK6 and CDC25A. *Genes Dev* **23**, 2388-2393, doi:23/20/2388 [pii] 10.1101/gad.1819009 (2009).
63 Xu, N., Papagiannakopoulos, T., Pan, G., Thomson, J. A. & Kosik, K. S. MicroRNA-145 regulates OCT4, SOX2, and KLF4 and represses pluripotency in human embryonic stem cells. *Cell* **137**, 647-658, doi:S0092-8674(09)00252-9 [pii] 10.1016/j.cell.2009.02.038 (2009).
64 Nicoloso, M. S. *et al.* Single-nucleotide polymorphisms inside microRNA target sites influence tumor susceptibility. *Cancer Res* **70**, 2789-2798, doi:0008-5472.CAN-09-3541 [pii] 10.1158/0008-5472.CAN-09-3541 (2010).
65 Saetrom, P. *et al.* A risk variant in an miR-125b binding site in BMPR1B is associated with breast cancer pathogenesis. *Cancer Res* **69**, 7459-7465, doi:0008-5472.CAN-09-1201 [pii] 10.1158/0008-5472.CAN-09-1201 (2009).
66 Chin, L. J. *et al.* A SNP in a let-7 microRNA complementary site in the KRAS 3' untranslated region increases non-small cell lung cancer risk. *Cancer Res* **68**, 8535-8540, doi:68/20/8535 [pii] 10.1158/0008-5472.CAN-08-2129 (2008).
67 Shimizu, M. *et al.* EGCG inhibits activation of the insulin-like growth factor (IGF)/IGF-1 receptor axis in human hepatocellular carcinoma cells. *Cancer Lett* (2007).
68 Lin, S. B. *et al.* Antisense oligodeoxynucleotides of IGF-II selectively inhibit growth of human hepatoma cells overproducing IGF-II. *J Biochem* **122**, 717-722 (1997).
69 Nakano, K. & Vousden, K. H. PUMA, a novel proapoptotic gene, is induced by p53. *Mol Cell* **7**, 683-694 (2001).
70 Yu, J., Zhang, L., Hwang, P. M., Kinzler, K. W. & Vogelstein, B. PUMA induces the rapid apoptosis of colorectal cancer cells. *Mol Cell* **7**, 673-682 (2001).
71 Bouillet, P. & Strasser, A. BH3-only proteins - evolutionarily conserved proapoptotic Bcl-2 family members essential for initiating programmed cell death. *J Cell Sci* **115**, 1567-1574 (2002).

72 Kim, C. H., Neiswender, H., Baik, E. J., Xiong, W. C. & Mei, L. Beta-catenin interacts with MyoD and regulates its transcription activity. *Mol Cell Biol* **28**, 2941-2951, doi:MCB.01682-07 [pii]
10.1128/MCB.01682-07 (2008).
73 North, S. *et al.* Regulation of cdc2 gene expression by the upstream stimulatory factors (USFs). *Oncogene* **18**, 1945-1955, doi:10.1038/sj.onc.1202506 (1999).
74 Cogswell, J. P., Godlevski, M. M., Bonham, M., Bisi, J. & Babiss, L. Upstream stimulatory factor regulates expression of the cell cycle-dependent cyclin B1 gene promoter. *Mol Cell Biol* **15**, 2782-2790 (1995).
75 Read, M. L., Clark, A. R. & Docherty, K. The helix-loop-helix transcription factor USF (upstream stimulating factor) binds to a regulatory sequence of the human insulin gene enhancer. *Biochem J* **295 ( Pt 1)**, 233-237 (1993).
76 Iynedjian, P. B. Identification of upstream stimulatory factor as transcriptional activator of the liver promoter of the glucokinase gene. *Biochem J* **333 ( Pt 3)**, 705-712 (1998).
77 Huang, S., Li, X., Yusufzai, T. M., Qiu, Y. & Felsenfeld, G. USF1 recruits histone modification complexes and is critical for maintenance of a chromatin barrier. *Mol Cell Biol* **27**, 7991-8002, doi:MCB.01326-07 [pii]
10.1128/MCB.01326-07 (2007).
78 Elmen, J. *et al.* LNA-mediated microRNA silencing in non-human primates. *Nature* **452**, 896-899 (2008).
79 Krutzfeldt, J. *et al.* Silencing of microRNAs in vivo with 'antagomirs'. *Nature* **438**, 685-689 (2005).
80 Murrell, A., Heeson, S. & Reik, W. Interaction between differentially methylated regions partitions the imprinted genes Igf2 and H19 into parent-specific chromatin loops. *Nat Genet* **36**, 889-893, doi:10.1038/ng1402
ng1402 [pii] (2004).
81 Hark, A. T. *et al.* CTCF mediates methylation-sensitive enhancer-blocking activity at the H19/Igf2 locus. *Nature* **405**, 486-489, doi:10.1038/35013106 (2000).
82 Kurukuti, S. *et al.* CTCF binding at the H19 imprinting control region mediates maternally inherited higher-order chromatin conformation to restrict enhancer access to Igf2. *Proc Natl Acad Sci U S A* **103**, 10684-10689, doi:0600326103 [pii]
10.1073/pnas.0600326103 (2006).
83 Maw, M. A. *et al.* A third Wilms' tumor locus on chromosome 16q. *Cancer Res* **52**, 3094-3098 (1992).
84 Yeh, A. *et al.* Chromosome arm 16q in Wilms tumors: unbalanced chromosomal translocations, loss of heterozygosity, and assessment of the CTCF gene. *Genes Chromosomes Cancer* **35**, 156-163, doi:10.1002/gcc.10110 (2002).
85 Veronese, R. V., Jessica Consiglio, Mario Acunzo, Laura Lupini, Taewan Kim, Manuela Ferracin,, Francesca Lovat, E. M., Veronica Balatti, Lucilla D'Abundo, Laura Gramantieri, Luigi Bolondi, & Yuri Pekarsky, D. P., Massimo Negrini and Carlo M. Croce. Mutated β-catenin evades a microRNA-dependent regulatory loop. *PNAS* **in press** (2011).
86 Reeve, A. E., Eccles, M. R., Wilkins, R. J., Bell, G. I. & Millow, L. J. Expression of insulin-like growth factor-II transcripts in Wilms' tumour. *Nature* **317**, 258-260 (1985).
87 Hu, Q. *et al.* Wt1 ablation and Igf2 upregulation in mice result in Wilms tumors with elevated ERK1/2 phosphorylation. *J Clin Invest* **121**, 174-183, doi:10.1172/JCI43772

43772 [pii] (2011).
88 Hoffman, B. & Liebermann, D. A. Apoptotic signaling by c-MYC. *Oncogene* **27**, 6462-6472, doi:onc2008312 [pii]
10.1038/onc.2008.312 (2008).
89 Sumi, T., Tsuneyoshi, N., Nakatsuji, N. & Suemori, H. Apoptosis and differentiation of human embryonic stem cells induced by sustained activation of c-Myc. *Oncogene* **26**, 5564-5576, doi:1210353 [pii]
10.1038/sj.onc.1210353 (2007).
90 Okuyama, H., Endo, H., Akashika, T., Kato, K. & Inoue, M. Downregulation of c-MYC protein levels contributes to cancer cell survival under dual deficiency of oxygen and glucose. *Cancer Res* **70**, 10213-10223, doi:0008-5472.CAN-10-2720 [pii]
10.1158/0008-5472.CAN-10-2720 (2010).
91 Wanzel, M., Herold, S. & Eilers, M. Transcriptional repression by Myc. *Trends Cell Biol* **13**, 146-150, doi:S0962892403000035 [pii] (2003).
92 Kahn, A. Transcriptional regulation by glucose in the liver. *Biochimie* **79**, 113-118, doi:S0300-9084(97)81501-5 [pii] (1997).
93 van Deursen, D., Jansen, H. & Verhoeven, A. J. Glucose increases hepatic lipase expression in HepG2 liver cells through upregulation of upstream stimulatory factors 1 and 2. *Diabetologia* **51**, 2078-2087, doi:10.1007/s00125-008-1125-6 (2008).
94 Kang, H. T. & Hwang, E. S. 2-Deoxyglucose: an anticancer and antiviral therapeutic, but not any more a low glucose mimetic. *Life Sci* **78**, 1392-1399, doi:S0024-3205(05)00698-3 [pii]
10.1016/j.lfs.2005.07.001 (2006).
95 Ralser, M. *et al.* A catabolic block does not sufficiently explain how 2-deoxy-D-glucose inhibits cell growth. *Proc Natl Acad Sci U S A* **105**, 17807-17811, doi:0803090105 [pii]
10.1073/pnas.0803090105 (2008).
96 Sanchez, A. P. & Sharma, K. Transcription factors in the pathogenesis of diabetic nephropathy. *Expert Rev Mol Med* **11**, e13, doi:S1462399409001057 [pii]
10.1017/S1462399409001057 (2009).
97 Dang, C. V. Rethinking the Warburg effect with Myc micromanaging glutamine metabolism. *Cancer Res* **70**, 859-862, doi:0008-5472.CAN-09-3556 [pii]
10.1158/0008-5472.CAN-09-3556 (2010).